NBS1 promotes the endonuclease activity of the MRE11-RAD50 complex by sensing CtIP phosphorylation

Anand, Roopesh ; Jasrotia, Arti ; Bundschuh, Diana ; Howard, Sean Michael ; Ranjha, Lepakshi ; Stucki, Manuel ; Cejka, Petr

Abstract: DNA end resection initiates DNA double-strand break repair by homologous recombination. MRE11-RAD50-NBS1 and phosphorylated CtIP perform the first resection step via MRE11-catalyzed endonucleolytic DNA cleavage. Human NBS1, more than its homologue Xrs2 in Saccharomyces cerevisiae, is crucial for this process, highlighting complex mechanisms that regulate the MRE11 nuclease in higher eukaryotes. Using a reconstituted system, we show here that NBS1, through its FHA and BRCT domains, functions as a sensor of CtIP phosphorylation. NBS1 then activates the MRE11-RAD50 nuclease through direct physical interactions with MRE11. In the absence of NBS1, MRE11-RAD50 exhibits a weaker nuclease activity, which requires CtIP but not strictly its phosphorylation. This identifies at least two mechanisms by which CtIP augments MRE11: a phosphorylation-dependent mode through NBS1 and a phosphorylation-independent mode without NBS1. In support, we show that limited DNA end resection occurs in vivo in the absence of the FHA and BRCT domains of NBS1. Collectively, our data suggest that NBS1 restricts the MRE11-RAD50 nuclease to S-G2 phase when CtIP is extensively phosphorylated. This defines mechanisms that regulate the MRE11 nuclease in DNA metabolism.

DOI: https://doi.org/10.15252/embj.2018101005

NBS1 promotes the endonuclease of the MRE11-RAD50 complex by sensing CtIP phosphorylation

Roopesh Anand[1], Arti Jasrotia[2], Diana Bundschuh[2], Sean Michael Howard[1], Manuel Stucki[2] and Petr Cejka[1,3]

Affiliations:

[1]Institute for Research in Biomedicine, Università della Svizzera italiana (USI), Faculty of Biomedical Sciences, Institute for Research in Biomedicine, Bellinzona, Switzerland

[2]Department of Gynecology, University of Zurich, Schlieren, Switzerland

[3]Department of Biology, Institute of Biochemistry, Eidgenössische Technische Hochschule (ETH) Zürich, Switzerland

Correspondence:

Petr Cejka, petr.cejka@irb.usi.ch. Institute for Research in Biomedicine, Università della Svizzera italiana, Via Vincenzo Vela 6, Bellinzona 6500, Switzerland. Telephone +41 91 820 03 61.

Abstract

DNA end resection initiates the repair of DNA breaks by homologous recombination. The MRE11-RAD50-NBS1 and phosphorylated CtIP perform the first resection step by MRE11-catalyzed endonucleolytic DNA cleavage. Human NBS1, unlike its homologue from *Saccharomyces cerevisiae*, is crucial for this process, highlighting complex mechanisms that regulate the MRE11 nuclease in high eukaryotes. Using a reconstituted system, we show here that NBS1, through its FHA and BRCT domains, functions as a sensor of CtIP phosphorylation. NBS1 then activates the MRE11-RAD50 nuclease through direct physical interactions with MRE11. In the absence of NBS1, MRE11-RAD50 exhibits a weaker nuclease activity, which requires CtIP but is not strictly dependent on its phosphorylation. This identifies at least two mechanisms how CtIP promotes MRE11: a phosphorylation-dependent mode through NBS1, and a phosphorylation-independent in the absence of NBS1. In support, we show that limited DNA end resection in the absence of the FHA and BRCT domains of NBS1 occurs *in vivo*. Collectively, our data suggest that NBS1 restricts the MRE11-RAD50 nuclease to S-G2 phase when CtIP is extensively phosphorylated. This defines mechanisms that regulate the MRE11 nuclease in DNA metabolism.

Introduction

The maintenance of genomic integrity is critically important as cells are constantly exposed to various genotoxic agents. DNA double-strand breaks (DSBs) represent a very deleterious lesion that is difficult to repair due to the loss of genetic information in both DNA strands. While unrepaired DSBs may result in cell death, their inaccurate repair can lead to mutagenesis and inappropriate chromosomal translocations (Ranjha et al., 2018). Cells possess two main mechanisms for DSB repair: end-joining pathways including Ku-dependent non-homologous end-joining (NHEJ) and Ku-independent microhomology-mediated end-joining (MMEJ), which are functional in any phase of the cell cycle and do not require a DNA template (Ranjha et al., 2018). The second mechanism is template-dependent homologous recombination (HR), which is generally restricted to the S-G2 phase of the cell cycle. The sister chromatid serves as an HR template in most cases in vegetative cells, explaining why recombination can only function in the cell cycle phases when sister chromatids are available (Ranjha et al., 2018). This is achieved by a regulatory mechanism involving cyclin-dependent kinases (CDKs), which phosphorylate key factors that function in the first step in the HR pathway termed DNA end resection (Huertas et al., 2008; Huertas and Jackson, 2009). Resection involves nucleolytic degradation of the 5'-terminated DNA strand at DSBs, leading to 3'-overhangs that are essential for the downstream steps in the recombination pathway. While limited DNA end resection may be involved in MMEJ, DNA that underwent extended resection is no longer ligatable and therefore unsuitable for end-joining. The decision whether and to which extent to resect DNA ends therefore regulates the pathway choice in DSB repair (Ranjha et al., 2018).

The MRE11-RAD50-NBS1 (MRN, in human cells) or Mre11-Rad50-Xrs2 (MRX, in yeast) complex has multiple key evolutionarily conserved functions to initiate and coordinate the repair of DSBs (Paull, 2010; Stracker and Petrini, 2011). This includes roles in both end-joining and homologous recombination repair pathways (Carney et al., 1998; de Jager et al., 2001; Moore and Haber, 1996; Paull and Gellert, 1998, 1999; Rass et al., 2009). Additionally, MRN promotes DNA end tethering and is required to signal the presence of DSBs *via* the ATM kinase (Carney et al., 1998; de Jager et al., 2001; Lee and Paull, 2005; Stewart et al., 1999; Usui et al., 2001; Williams et al., 2008). This is achieved by a conserved interaction between the MRN subunit NBS1 (Xrs2 in *S. cerevisiae*) and ATM (Tel1 in yeast). ATM in turn phosphorylates hundreds of protein targets that regulate the response to DSBs. Beyond ATM, NBS1 also interacts with MDC1, which binds phosphorylated proteins including H2AX (γH2AX) to amplify the DNA damage signaling

beyond the vicinity of the DSB (Goldberg et al., 2003). In recombination, the MRN complex has a direct role in DNA end resection mediated by the MRE11 nuclease in the S-G2 phase of the cell cycle. MRE11 is likely the first nuclease to resect DSBs, which is particularly important for the processing of breaks with secondary DNA structures or protein adducts such as stalled topoisomerases or Ku (Anand et al., 2016; Deshpande et al., 2016; Reginato et al., 2018; Shibata et al., 2014; Wang et al., 2017). The current models posit that resection by MRE11 is initiated by an endonucleolytic DNA cleavage internal to the DSB past the protein block, followed by 3'→5' exonucleolytic degradation back toward the DNA end (Cannavo and Cejka, 2014; Garcia et al., 2011; Keeney and Kleckner, 1995; Neale et al., 2005; Shibata et al., 2014). The endonucleolytic cleavage sites also represent entry sites for processive DNA end resection nucleases that function downstream of MRN in the 5'→3' direction, including EXO1 and DNA2 (Gravel et al., 2008; Mimitou and Symington, 2008; Nimonkar et al., 2011; Zhu et al., 2008). The MRN nuclease furthermore likely functions to promote MMEJ independently of the cell cycle, which to date remains very poorly defined (Deng et al., 2014; Ma et al., 2003; Rahal et al., 2010; Sharma et al., 2015; Taylor et al., 2010; Truong et al., 2013).

The processing of protein-blocked DSBs is an evolutionarily conserved capacity of MRE11 homologues and their co-factors. In bacteria, the MRE11-RAD50-like SbcC-SbcD complex endonucleotically cleaves DNA near blocked DNA ends (Connelly et al., 2003). Eukaryotic cells possess a third member of the MRE11-RAD50 complex, NBS1/Xrs2, as well as CtIP/Sae2, which function as a co-factors of the MRE11 nuclease in resection (Carney et al., 1998; Sartori et al., 2007). In *S. cerevisiae*, Sae2 phosphorylated by CDK and other kinases has a critical function to promote the Mre11-Rad50 endonuclease near protein blocks (Cannavo and Cejka, 2014; Huertas et al., 2008; Reginato et al., 2018; Wang et al., 2017), while Xrs2 *per se* is not essential for the DNA clipping reaction (Oh et al., 2016), but may have a stimulatory function (Wang et al., 2017). It has been demonstrated that Xrs2 is responsible for the nuclear import of the MRX complex (Carney et al., 1998; Tsukamoto et al., 2005). When this function was bypassed by placing the nuclear localization signal on Mre11, Xrs2 became dispensable for the Mre11-Rad50-dependent functions in resection also *in vivo* (Oh et al., 2016). In contrast, Xrs2 *per se* was required for DNA-damage signaling function of the MRX complex (Oh et al., 2016). In humans, both CtIP, when phosphorylated by CDK, and NBS1 promote the MRE11-RAD50 endonuclease (Anand et al., 2016; Deshpande et al., 2016). The differential requirement for NBS1/Xrs2 between budding yeast and humans likely reflects the need for more complex regulatory mechanisms to control the MRE11 nuclease in high eukaryotes. How NBS1 performs this function however remains poorly characterized.

Beyond DSB processing, unscheduled DNA degradation by MRE11 at stalled DNA replication forks may be responsible for the toxicity associated with defects in BRCA1 or BRCA2, further highlighting the importance to understand how MRE11 nuclease is regulated in human cells (Feng and Jasin, 2017; Mijic et al., 2017; Ray Chaudhuri et al., 2016; Schlacher et al., 2011).

Human NBS1 consists of 754 amino acids. The N-terminus contains forkhead-associated domain (FHA) and tandem BRCA1 C-terminal (BRCT) motifs (BRCT1 and BRCT2), which bind phosphorylated proteins including CtIP and MDC1 (Wang et al., 2013; Williams et al., 2009). At its C-terminal part, NBS1 contains ATM and MRE11 interaction sites, as well as three potential nuclear localization signals that promote the nuclear import of MRN (Carney et al., 1998; Falck et al., 2005; Nakada et al., 2003; Tsukamoto et al., 2005; You et al., 2005). The FHA domain of *S. cerevisiae* Xrs2 binds phosphorylated Sae2, although this capacity appears to be mostly dispensable for DNA end resection *in vitro* and *in vivo* (Liang et al., 2015; Oh et al., 2016). Structural and biochemical characterization of MRN in *Schizosaccharomyces pombe* revealed that it also binds phosphorylated Ctp1, an ortholog of CtIP/Sae2 in *S. pombe*, through the FHA motif of Nbs1 (Lloyd et al., 2009; Williams et al., 2009). A point mutation that affects this interaction resulted in hypersensitivity to ionizing radiation and camptothecin, as well as impaired Ctp1 enrichment at DSBs (Williams et al., 2009). Similarly in human cells, CtIP phosphorylated by CDK at multiple sites in the center of the protein binds the FHA-BRCT domains of NBS1, which is important for DNA end resection (Hari et al., 2010; Wang et al., 2013). However, this CDK-dependent phosphorylation was also important for the subsequent modification of T859 by ATM that is required for resection *in vivo*. Phosphomimetic T859E could partially bypass the requirement for the phosphorylation of CtIP at CDK sites that mediate its interaction with the FHA-BRCT domains of NBS1, raising questions whether these domains are required for resection *per se*, or only serve as a platform to help phosphorylate CtIP at T859 (Wang et al., 2013). Likewise, mutations in FHA-BRCT abrogate the interaction of NBS1 with MDC1, which may have an indirect effect on resection as a result of disrupted signaling (Goldberg et al., 2003). Because of the multiple functions of the MRN complex and potential pleiotropic phenotypes associated with NBS1 defects, the interpretation of cell-based resection assays with NBS1 variants is challenging.

Here, we primarily employ *in vitro* reconstituted reactions to define the function of NBS1 in DNA end resection by MRN-CtIP. We show that both FHA and BRCT domains of NBS1 promote resection by MRE11 through interacting with phosphorylated CtIP. When NBS1 senses that CtIP is phosphorylated, it promotes resection by a mechanism that is

dependent on its interaction with MRE11. This is in agreement with a recent study showing that an NBS1 fragment containing the MRE11 biding site but not FHA-BRCT rescues embryonic lethality of NBS1-deficient mice (Kim et al., 2017). Importantly, we identify an NBS1-independent DNA cleavage activity of MRE11-RAD50 and CtIP. Although less efficient than the resection capacity of the MRN-CtIP holocomplex, the NBS1-independent activity is promoted by CtIP but surprisingly does not require its phosphorylation. Accordingly, we find limited CtIP- and MRE11-dependent but NBS1-independent DSB resection activity *in vivo*. These results suggest that a mechanism that interferes with the function of NBS1 might allow limited resection in the absence of CDK-dependent modification of CtIP, which might be relevant for understanding MRE11 nuclease functions in G1.

Results:

NBS1 in trans promotes endonucleolytic cleavage by MRE11-RAD50 and pCtIP

Previously, we showed that phosphorylated CtIP (pCtIP) promotes the clipping of the 5'-terminated DNA strand near protein blocked DSBs by the MRE11 nuclease within the MRE11-RAD50-NBS1 (MRN) complex (Anand et al., 2016). This reaction is believed to initiate DNA end resection by MRN. The dsDNA clipping efficiency of MRE11-RAD50 (MR) was strongly reduced compared to MRN, showing that NBS1 has an important function to stimulate this activity, in contrast to its yeast Xrs2 homologue, which is largely dispensable (Anand et al., 2016; Deshpande et al., 2016; Oh et al., 2016). To define the function of NBS1 in the regulation of the MRE11 nuclease in the human system, we expressed and purified NBS1, as well as MR, MRN complexes and pCtIP in S*podoptera frugiperda* 9 (*Sf*9) insect cells (Figs 1A and EV1A-C).

NBS1 was purified by affinity chromatography by utilizing maltose binding protein (MBP) and 10x histidine (his) tags, located at N- and C-termini, respectively. As the removal of the MBP tag by PreScission protease cleavage was not very efficient (Fig EV1D), this step was omitted during the final purification (Fig 1A). MBP-NBS1-his added in *trans* promoted dsDNA clipping by MR and pCtIP (Fig 1B and C). This was indistinguishable from DNA cleavage by pCtIP and MRN purified as a complex, where NBS1 is untagged, both in terms of cleavage positions and efficiency (Fig 1B and C). Therefore, the affinity tags did not affect the stimulatory function of NBS1 on dsDNA clipping by MR and pCtIP *in vitro*. To further confirm this, we note that a treatment of MBP-NBS1 with PreScission protease, which cleaves ~50% of the MBP tag off NBS1, did not affect dsDNA clipping efficiency (Fig EV1D and E). Finally, FLAG-NBS1-his construct promoted DNA cleavage similarly as MBP-NBS1-his (Fig EV1F and G). In summary, we conclude that MBP-NBS1-his (hereafter NBS1 for brevity) added in *trans* promotes the capacity of MR and pCtIP ensemble to clip 5'-terminated DNA in the vicinity of protein blocks.

FHA and BRCT domains of NBS1 are important for the processing of protein blocked DSBs, while its interaction with MRE11 is essential

NBS1 mediates physical interactions of the MRN complex with ATM, BRCA1, BLM, MDC1, CtIP and possibly other factors (Carney et al., 1998; Chen et al., 2008; Goldberg et al., 2003; Hari et al., 2010; Spycher et al., 2008; Stewart et al., 1999; Wang et al., 2013; Wang et al., 2000; Williams et al., 2008). Out of these, the interactions with CtIP and

MDC1 are at least in part phosphorylation-dependent. To specifically define the functional interaction of NBS1 with MR and pCtIP in resection, we employed our *in vitro* reconstituted system (Anand et al., 2016). To this point, we prepared NBS1 variants lacking particular domains or carrying mutations specifically affecting known interactions with the MR and pCtIP ensemble (Fig 2A and B), and assayed them in nuclease assays to determine their effect on the MRE11 endonuclease.

We first varied the concentrations of wild type NBS1 in reactions with MR and pCtIP. While weak NBS1-independent DNA cleavage was observed (Fig 2C and D), we found that less than equimolar concentrations of NBS1 compared to the MR complex were sufficient for maximal DNA clipping activity (Fig 2C and D). We next tested various NBS1 fragments lacking FHA, BRCT or both domains (Figs 2E and EV2A). As phosphorylation of CtIP is required for resection (Huertas and Jackson, 2009), and the MRN complex primarily binds phosphorylated CtIP *via* the FHA and BRCT domains of NBS1 (Figs 2F and G)(Wang et al., 2013; Williams et al., 2009), a strong defect in resection was anticipated. As shown in Fig 2E, a deletion of either FHA or BRCT domain in NBS1 had only a minor effect on resection *in vitro*, while elimination of both domains significantly reduced but not eliminated resection. Similar effects were observed with the NBS1 RRHK variant, carrying four point mutations (R28A, R43A, H45A in FHA and K160M in BRCT1, Fig 2A)(Wang et al., 2013). The RRHK mutations decreased the phosphorylation-dependent interaction of NBS1 with phosphorylated MDC1 (Hari et al., 2010), as well as with pCtIP (Fig 2F), which led to a dramatic DNA end resection defect *in vivo*, as scored by single-strand annealing reporter assay (Hari et al., 2010; Wang et al., 2013). Despite the strong physical interaction between the FHA and BRCT domains of NBS1 and pCtIP (Fig 2F), which is dependent on CtIP phosphorylation (Fig 2G), we conclude that both domains of NBS1 are important, but not essential for the DNA clipping activity *in vitro* together with MR and pCtIP. Furthermore, NBS1 (335-754) exhibited similar stimulatory activity to NBS1 (622-754), revealing that the central NBS1 region (residues 335-621) is dispensable for MR and pCtIP-mediated resection, despite this region mediated residual interaction with pCtIP (Fig 2E and F, and H).

It has been demonstrated that the MRE11-RAD50 complex directly interacts with NBS1 *via* the MRE11-interaction region (MIR) within the C-terminal part of NBS1, with the most important motif located between residues 684-690 of NBS1 (Desai-Mehta et al., 2001; Kim et al., 2017; Schiller et al., 2012). This interaction facilitates MRN entry into the nucleus as only NBS1 contains the nuclear localization sequence. Therefore, *in vivo* experiments with mutated MIR of NBS1 cannot easily distinguish effects related to

impaired nuclear entry from direct effects on the biochemical activities of the MR complex. Using our *in vitro* system, where any effects on nuclear import are irrelevant, we observed that in contrast to the FHA and BRCT domains, the MRE11 interaction region in NBS1 was absolutely essential for the stimulatory function of NBS1 on the MRE11-RAD50 endonuclease in conjunction with pCtIP (Figs 2H and EV2B). Specifically, the NBS1 (1-692) fragment lacking the very C-terminal region of NBS1, but possessing MIR, exhibited similar activity as full-length NBS1 (Figs 2H and EV2A). However, additional shortening by 9 residues comprising MIR (residues 684-692) completely eliminated the stimulatory activity (Figs 2H and EV2A and B). Likewise, the internal deletion of MIR (residues 684-690) totally abolished NBS1 function in DNA clipping, even at high concentrations (Figs 2H and EV2B and C). In accord with previous studies (Desai-Mehta et al., 2001; Schiller et al., 2012), we observed a dramatic reduction of the MRE11 and NBS1 physical interaction when NBS1 ΔMIR variant was used in pulldown experiments instead of wild type NBS1 (Fig EV2D and E). In summary, the NBS1-dependent interaction with MRE11-RAD50, more than that with pCtIP, is important for the endonuclease activity of the MRE11-RAD50 and pCtIP nuclease ensemble.

In the absence of pCtIP, NBS1 promotes MR cleavage independently of its FHA and BRCT domains

Recently, it has been shown that NBS1 alone is capable of stimulating the endonucleolytic activity of MR on protein-blocked dsDNA, independently of CtIP (or pCtIP)(Deshpande et al., 2016). Although CtIP-independent DNA end resection does not likely occur *in vivo* (Sartori et al., 2007), we used the *in vitro* assay to learn more about the function of NBS1. To this point, we employed our NBS1 mutants in an MR-dependent nuclease assay with streptavidin-blocked dsDNA. In contrast to the assays that included pCtIP, the reactions were incubated for 2 h instead of 30 min to compensate for the lower cleavage efficacy in the absence of pCtIP. We observed that all NBS1 fragments containing MIR stimulated the clipping activity of MR almost indistinguishably, irrespectively of FHA and BRCT domains (Figs 3A and B, and EV3A). This included the short NBS1 (622-754) fragment containing 133 residues, which stimulated the endonucleolytic cleavage to the same extent as full-length wt NBS1. Conversely, NBS1 fragments lacking MIR did not at all promote MR (Figs 3A and B, and EV3A). Very similar results were obtained using circular ssDNA as a substrate, which forms a variety of secondary DNA structures (Fig 3C and D). However, as noted previously, we believe that the cleavage of dsDNA near protein blocks is a better model for the resection reactions taking

place in cells (Fig EV3B-F) (Anand et al., 2016; Chen et al., 2005; Deshpande et al., 2014). In summary, we show that in the absence of pCtIP, the phosphoprotein binding domains of NBS1 become dispensable for resection *in vitro*. This supports a model for resection in wild type cells, where the FHA-BRCT domains of NBS1 promote resection by binding phosphorylated CtIP, and NBS1 in turn activates the MR complex by interacting with MRE11.

BRCT and FHA domains of NBS1 are important but not absolutely essential for resection *in vivo*

To verify the physiological significance of our data, we first designed an NBS1 complementation system in U2OS cells to define the requirement of the FHA and BRCT domains of NBS1 for DNA end resection *in vivo*. The expression of endogenous wild type NBS1 was suppressed with siRNA, and siRNA resistant myc-tagged NBS1 variants were expressed from a construct containing doxycycline-inducible promoter stably integrated into chromosomal DNA (Fig 4A). Downregulation of endogenous NBS1 led to cellular sensitivity to ionizing radiation, retention of MRE11 in the cytoplasm and a DNA end resection deficiency, as anticipated (Figs 4B-G, and EV4A and B). Expression of wt myc-tagged NBS1 overcame these defects, verifying the functionality of the complementation system (Figs 4B-G, and EV4A and B).

To test for the involvement of the FHA and BRCT domains of NBS1 in resection, we expressed wt NBS1, NBS1 R28A (a point mutation in the FHA domain), NBS1 K160M (a point mutation in the BRCT domain), or the NBS1 R28A K160M double mutant (DM) (Cerosaletti and Concannon, 2003; Hari et al., 2010; Wang et al., 2013). These cell lines were treated with siNBS1 for 72 h to knock down endogenous NBS1 (Fig 4A). For the last 24 h, the expression of the complementing NBS1 variant was induced by the addition of doxycycline. Cells were then irradiated (5 Gy) and DNA end resection was scored by automated counting of BrdU foci in ssDNA under non-denaturing conditions or by counting of RPA2 foci (Fig 4D-G). The mutation in either FHA or BRCT domain led to an intermediate defect in DNA end resection in both resection assays. The NBS1 R28A K160M double mutant led to a more severe, but not complete abrogation, comparable to NBS1 depletion (Fig 4D-G). Both FHA and BRCT domains thus individually promote, but are not absolutely essential, for the DNA end resection function of NBS1 in full agreement with our biochemical analysis.

Depletion of CtIP brought about a more severe defect than that of NBS1, and nearly completely eliminated BrdU or RPA2 foci upon IR (Fig 4D-G). This confirmed that CtIP is essential for almost all DNA end resection activity, as observed previously by others (Sartori et al., 2007). Furthermore, the depletion of NBS1 brought about lesser defects compared to CtIP depletion in homologous recombination as scored by a DR-GFP reporter assay (Fig EV4C-D). Finally, depletion of NBS1 did not completely eliminate single-strand annealing (SSA)(Fig 4I), which is a good readout for extensive DNA end resection (Stark et al., 2004). We also note that the residual SSA activity observed in the reporter assay without NBS1 was MRE11 dependent (Fig 4I).

The depletion of NBS1 by siRNA may not be complete and may thus explain the residual resection we observed. To this point, using CRISRP/Cas9, we constructed a U2OS hypomorphic NBS1ΔN cell line that expresses low levels of a C-terminal fragment of NBS1, which completely lacks the FHA and BRCT domains (Fig EV4F). Similarly as in mice (Kim et al., 2017), where a C-terminal fragment of NBS1 rescued viability and ATM activation, the NBS1ΔN cells were viable and grew normally in the absence of exogenous DNA damage (data not shown). MRE11 was partially retained in the cytoplasm in this cell line, most likely owing to the low expression level of the hypomorphic NBS1 allele that may not be sufficient to fully localize MRE11 in the nucleus (Fig EV4G). However, stable expression of recombinant wild type or R28A K160M mutated NBS1 (C-terminally tagged with the monomeric GFP analogue mNeonGreen), fully restored MRE11 nuclear localization (Fig EV4F-G). DNA end resection in the NBS1ΔN cell line was similarly compromised as in the cells depleted from NBS1 by siRNA (Fig EV4E). Consistent with our siRNA-based complementation system, stable expression of wild type NBS1 in the NBS1ΔN cell line efficiently restored DNA end resection activity, whereas expression of the R28A K160M double mutant (DM) did not, indicating that even though MRE11 nuclear localization is restored by DM NBS1, resection activity is not (Fig 4H). This shows that in contrast to yeast Xrs2, NBS1 has functions in DNA end resection beyond mediating nuclear localization of MRE11 and RAD50. Interestinlgy, both in WT and DM expressing cells residual resection activity is dependent on CtIP (Fig 4H), thus suggesting that CtIP can stimulate resection independently of NBS1 also *in vivo*. Together, we demonstrated that limited CtIP-dependent DNA end resection *in vivo* can occur without the FHA-BRCT domains of NBS1.

Depletion of NBS1 impairs nuclear entry of the MR complex (Fig 4B). To circumvent this problem, we used the NBS1 knockout cell line that was complemented with NBS1 R28A

K160M double mutant, which is compromised in its interaction with pCtIP, but proficient in mediating nuclear import of MR (Cerosaletti and Concannon, 2003; Hari et al., 2010; Wang et al., 2013). Under these conditions, when NBS1 fails to interact with CtIP, CtIP was still responsible for most of the residual DNA end resection activity (Fig EV4F). Together, we demonstrate that limited Mre11 and CtIP-dependent DNA end resection can occur in the absence of NBS1 *in vivo*.

Phosphorylation of CtIP is partially dispensable for stimulation of MR in the absence of NBS1

NBS1 specifically binds phosphorylated CtIP (Fig 2G), and phosphorylation of CtIP by CDKs is key for stimulating the MRN endonuclease activity (Anand et al., 2016). Therefore, the observation that limited CtIP-dependent resection can occur without the FHA-BRCT domains of NBS1 raised the question whether phosphorylation of CtIP is required under these conditions. In Figure 2CD, we observed weak NBS1-independent resection *in vitro*. To better define the mechanism of this reaction, we modified our biochemical assay conditions and employed the extended reaction incubation time (2 h) to improve the detection limit. As shown in Fig 5A and B, we observed that pCtIP stimulated dsDNA cleavage by MR in the absence of NBS1 in a concentration-dependent manner. Our previous experiments established NBS1 as a reader of CtIP phosphorylation, and the NBS1-independent reaction thus identifies a separate mechanism for CtIP-facilitated stimulation of MR. Next, we set out to test whether phosphorylation of CtIP was required. We treated or mock-treated pCtIP with λ phosphatase. As shown previously (Anand et al., 2016), we observed that only pCtIP (i.e. mock-treated), but not λCtIP, stimulated DNA cleavage by MRN in a concentration-dependent manner (Fig 5C-E). In contrast, we observed a robust stimulation of MR-dependent DNA clipping by both phosphorylated and λ phosphatase-treated CtIP (Fig 5C-E). Very similar results were obtained in kinetic assays: with MRN, pCtIP was ~7-fold more efficient in promoting the DNA cleavage compared to λCtIP; with MR, the difference was only ~1.5-fold (Figs 5F and G, and EV5A). Therefore, NBS1 appears to restrict DNA cleavage by MR to conditions when CtIP is phosphorylated. Without NBS1, the MR cleavage is more promiscuous and can occur without CtIP phosphorylation.

One of the key residues in CtIP that needs to be phosphorylated by CDKs to allow DNA end resection during S-phase is T847, which maps to a conserved region that is equivalent to S267 of *S. cerevisiae* Sae2 (Huertas et al., 2008; Huertas and Jackson, 2009). Non-phosphorylatable substitution of T847 with alanine, resulting in T847A mutation,

renders pCtIP incapable to promote DNA end resection (Anand et al., 2016; Huertas and Jackson, 2009). Unexpectedly, we observed that the pCtIP T847A mutant was incapable to promote both MR and MRN (Fig 5H and I). This suggested that the T847A variant is likely structurally impaired, beyond being non-phosphorylatable at the key CDK consensus site. Alternatively, the failure of pCtIP T847A to promote MR, in contrast to λCtIP, may stem from the presence of other phosphorylated residues in pCtIP T847A that have an inhibitory function together with MR. To test for this scenario, we treated pCtIP T847A with λ-phosphatase, and observed a minor, yet statistically significant, rescue of DNA clipping by MR (Fig EV5B and C). As wt λCtIP is still more efficient in promoting the MR endonuclease than λCtIP T847A, the T847A substitution in pCtIP likely brings about structural changes within the conserved CtIP region that affect CtIP activity beyond mimicking a non-phosphorylated threonine. Our conclusion that the T847A mutation might bring about structural defects in the conserved domain of CtIP prevented us to test whether non-phosphorylatable CtIP promotes DNA end resection in the absence of NBS1 *in vivo*.

Together, our results demonstrate that NBS1, as CtIP, is a co-factor that stimulates the DNA cleavage efficacy of the MR complex. Reactions with MRN require CtIP phosphorylation, and lead to extensive DNA end resection activity that is required for homologous recombination and SSA. In contrast in the absence of NBS1, CtIP phosphorylation is partially dispensable for the DNA cleavage activity of the MR complex.

The physical interaction of MRE11 and RAD50 with CtIP does not require CtIP phosphorylation

Our observation that CtIP was able to stimulate the DNA cleavage capacity of the MR complex prompted us to define physical interactions between MRE11, RAD50 and phosphorylated or non-phosphorylated CtIP. CtIP is known to interact with all subunits of the MRN complex (Chen et al., 2008; Sartori et al., 2007; Williams et al., 2009; Yuan and Chen, 2009); in accord, we detected direct interactions between pCtIP/CtIP and both MRE11 and RAD50 (Fig 6A and B). While phosphorylation of CtIP was absolutely required for its interaction with NBS1 (Fig 2G), this was not the case for MRE11 and RAD50. In contrast, λ phosphatase-treated CtIP interacted with both MRE11 and RAD50 even better than pCtIP (Fig 6A and B). We cannot exclude that the apparent increase in protein-protein interaction was due to aggregation of non-phosphorylated CtIP, or that our preparation of pCtIP contained phosphorylated residues that are not normally modified *in vivo*, which could inhibit the interaction with MRE11 and RAD50. Nevertheless,

NBS1 is mostly responsible for the interaction between the MRN complex and pCtIP, and phosphorylation of CtIP is indispensable for this interaction (Fig 6C). The comparatively weaker interactions of MRE11 and RAD50 with CtIP do not require CtIP phosphorylation.

NBS1 within the MRN-pCtIP ensemble promotes endonucleolytic activity by promoting access into dsDNA

NBS1 is known to enhance ATP-driven dsDNA melting capacity of the MRN complex, resulting in the promotion of endonucleolytic cleavage of DNA near secondary structures (Paull and Gellert, 1999). The differential role of DNA melting in the exonucleolytic vs. endonucleolytic mechanism of DNA degradation by MRE11 allowed Tainer and colleagues to prepare MRE11 inhibitors specific for its exo- vs. endonuclease activity (Shibata et al., 2014). The endonuclease-specific PFM03 was designed to block a hypothesized ssDNA binding pocket at a location separate from the active site, in accord with the notion that dsDNA melting is prerequisite for the endonucleolytic cleavage by MR (Lafrance-Vanasse et al., 2015; Shibata et al., 2014). In addition to the endonucleolytic cleavage of secondary DNA structures reported previously (Shibata et al., 2014), we observed that the PFM03 inhibitor also efficiently reduced the clipping of protein-blocked DSBs by the MRN complex in conjunction with pCtIP, while PFM39, an exonuclease inhibitor, did not (Fig EV6A and B). This is in agreement with the observation that the PFM03 inhibitor blocks the first step in DNA end resection *in vivo* (Shibata et al., 2014).

To learn more about the involvement of NBS1 in the DNA clipping reaction, we employed a substrate similar to that used by Paull and colleagues that contains a preexisting nick in the strand opposite to the anticipated cleavage site (Deshpande et al., 2016). We reasoned that the pre-existing nick may reduce the energy required to melt dsDNA, and therefore allow the MR complex to cleave DNA without NBS1. To this point, we performed kinetic analyses with both nicked and non-nicked DNA substrates, which had phosphorothioate bonds at the 3'-ends to prevent exonucleolytic DNA degradation by Mre11 (or MR/MRN). We observed that MRE11 alone had no endonuclease activity on any of the substrates tested, with or without CtIP, as expected (Fig 7A and B, lanes 3 and 6). As previously, NBS1 promoted the cleavage of the non-nicked DNA substrate (Fig 7A and C) and pCtIP was essential. In contrast, NBS1 was dispensable when nicked DNA substrate was used (Fig 7B, D and E). Under these conditions, pCtIP provided a moderate stimulatory effect, with or without NBS1 (Fig 7B, D and E). The endonuclease activity was promoted by a nick or a gap in the top strand, as a substrate lacking the top left

oligonucleotide was not endonucleolytically cleaved by MR-CtIP or MRN-pCtIP (Fig EV7C), and the DNA cleavage was directed by a protein block (Fig EV7D). Together, our results suggest that NBS1, and to a lesser extent pCtIP, is dispensable for the endonucleolytic DNA cleavage in case of a pre-existing nick opposite to the cleavage site. We hypothesize that a nick allows the MR complex to melt into the dsDNA molecule and the function of NBS1 to melt dsDNA thus becomes partially dispensable.

Discussion

The MRE11 nuclease plays critical functions at DSBs as well as at stalled, collapsed or reversed replication forks (Stracker and Petrini, 2011). Scheduled activation of the MRE11 nuclease is important for both homologous recombination and microhomology-mediated end-joining DSB repair pathways. In contrast, inappropriate MRE11 nuclease may result in illegitimate recombination leading to genome rearrangements or excessive DNA degradation at challenged replication forks leading to cell lethality in certain genetic backgrounds (Schlacher et al., 2011). Therefore, the activity of the MRE11 nuclease must be finely controlled and restricted to situations when it is appropriate for genome stability maintenance. MRE11 is a 3'→5' exonuclease on its own (Paull and Gellert, 1998). In complex with RAD50 and other co-factors, MRE11 can cleave dsDNA endonucleolytically (Paull and Gellert, 1998, 1999). It is believed that the processing of DSBs or reversed DNA replication forks is initiated by the endonucleolytic cleavage of the 5'-terminated DNA strand by MRE11 and co-factors (Cannavo and Cejka, 2014; Garcia et al., 2011; Lemacon et al., 2017; Neale et al., 2005). Eukaryotic cells possess two key regulators of the MR nuclease complex: CtIP/Sae2 and NBS1/Xrs2. In yeast, phosphorylated Sae2, but not Xrs2 is required for the endonucleolytic DNA cleavage by MR (Oh et al., 2016). In humans, both NBS1 and phosphorylated CtIP promote the activity of the MR endonuclease, revealing that NBS1 is a regulator of MRE11 that is employed specifically in high eukaryotes (Anand et al., 2016; Deshpande et al., 2016). In this study, we define the mechanism by which NBS1 regulates the MRE11 endonuclease using primarily a reconstituted *in vitro* system.

We show that NBS1 functions as a sensor of CtIP phosphorylation, which allows the MRE11 nuclease activation only when CtIP is phosphorylated (Fig. 8A-C). The FHA and BRCT are highly conserved phosphoprotein binding domains, which mediate the physical interaction of NBS1 with phosphorylated CtIP and both these domains promote resection *in vitro* as well as *in vivo*. Once NBS1 senses that CtIP is phosphorylated, it activates the MR endonuclease, which is dependent on a direct physical interaction between

NBS1 (residues 684-692) and MRE11 (Fig 8A). We found that the FHA and BRCT domains of NBS1 are important, but not absolutely essential for the MR and pCtIP-dependent cleavage of dsDNA near protein blocks. More than the FHA-BRCT domains, the short region within the C-terminus of NBS1 that interacts with MRE11 is absolutely required for the NBS1 function to promote the MR complex in conjunction with pCtIP. In support of this model, we observed a residual NBS1-dependent, but pCtIP-independent nuclease activity of the MR complex *in vitro* (Fig 8C). Without phosphorylated CtIP, NBS1 still promotes DNA cleavage by MR. In this case, the FHA-BRCT domains of NBS1 were entirely dispensable, while the MRE11 interaction region was required. Nevertheless, while this *in vitro* reaction informs us about the underlying mechanism, we believe that CtIP-independent resection does not occur *in vivo*, as depletion of CtIP entirely eliminated resection in cells in all assays tested (Fig 4)(Sartori et al., 2007).

Next, we observed that in the absence of NBS1, CtIP still promotes the endonuclease of MR, albeit to a lesser extent. This was observed *in vitro* (Fig 5), as well as in cells upon NBS1 depletion or gene editing that eliminated the FHA and BRCT domains of NBS1 (Fig 4). Strikingly, CtIP phosphorylation was not strictly required in the absence of NBS1 (Figs 5C-G and 8B). While this result is in agreement with the NBS1 function as a sensor of CtIP phosphorylation, the result was nevertheless surprising, as it revealed fundamental differences between the budding yeast and human systems. In yeast, Sae2 phosphorylation regulates its physical interaction with Rad50 (Cannavo et al., 2018), in addition to Xrs2. Therefore, even in the absence of Xrs2, Sae2 phosphorylation is still fully required for the stimulation of the Mre11-Rad50 endonuclease. Using human proteins instead, we found that the phosphorylation of CtIP was largely but not completely dispensable for the activation of MR in the absence of NBS1. This result might help explain how CtIP promotes limited resection in G1. It is well established that CDK and ATM-dependent phosphorylation of CtIP is necessary for the activation of extended resection and hence homologous recombination in S-G2 (Huertas et al., 2008; Huertas and Jackson, 2009). Nevertheless, CtIP likely activates MRE11 in MMEJ, which is not restricted to S-G2 and requires only minimal resection (Averbeck et al., 2014; Dutta et al., 2017; Sharma et al., 2015; Truong et al., 2013). In G1, CtIP is phosphorylated at S327, which mediates its interaction with BRCA1, but the G1 form of CtIP will likely lack other phosphorylation modifications that occur in S-G2 (Biehs et al., 2017; Yu and Chen, 2004). We speculate that this form of CtIP could promote the MR complex in case the NBS1 function is inhibited. However, we were unable to test this hypothesis directly, as CtIP variant that is non-phosphorylatable at the key CDK site appears to be impaired beyond mimicking a non-phosphorylated residue (Fig 5H and I).

While MRE11 and RAD50 form a constitutively interacting dimer of dimers complex, there are conflicting reports about the stoichiometry of NBS1 within the MRN complex (Paull and Gellert, 1999; Schiller et al., 2012; Trujillo et al., 1998). Furthermore, it has been reported that the physical interaction of NBS1 with MR may be differentially regulated in G1 vs. S-G2, upon DNA damage or at various subcellular locations, such as at telomeres (Limbo et al., 2018; Zhou et al., 2017; Zhu et al., 2000). Specifically, the MR complex was shown to localize to DSBs in the absence of NBS1 (Limbo et al., 2018), and NBS1 co-localized with MR to telomeres in S but not during interphase (Zhu et al., 2000). Finally, we show here that DNA end resection was strongly reduced but not completely eliminated in the absence of NBS1 in cells, despite the reduced nuclear import of MR, showing that NBS1 may not be an obligate component of the resection machinery under all conditions. Our data suggest that a reduction of the MR interaction with NBS1 may allow the complex to respond to non-phosphorylated or differently phosphorylated CtIP. It is additionally possible that NBS1's function as a sensor of CtIP phosphorylation might be regulated by posttranslational modifications of NBS1 (which is heavily phosphorylated) and/or by other proteins that could regulate NBS1 function. More research is needed to fully understand the mechanisms of resection in G1, and the involvement of MRN and CtIP proteins in this context. Together, our results demonstrate that the MRE11-RAD50 endonuclease is on its own restricted and becomes fully functional in the presence of NBS1 and phosphorylated CtIP. By regulating these co-factors through multiple mechanisms, cells can fine-tune the function of the MR endonuclease to optimally promote genome stability in various physiological contexts.

Material and Methods

Cloning, expression and purification of recombinant proteins

Recombinant MRN, MR and phosphorylated CtIP were expressed in insect *Spodoptera frugiperda* (*Sf*) 9 cells and purified by affinity and ion exchange chromatography as described previously (Anand et al., 2018; Anand et al., 2016). MBP-NBS1-his and its variants, as well as MRE11-his and FLAG-NBS1-his were expressed in *Sf*9 cells and purified as described in detail in supplementary information. To prepare the pFB-MBP-NBS1-his expression construct, NBS1 was amplified from pTP36 (a kind gift from Tanya Paull, University of Texas) by PCR using primers NBS1_F and NBS1_R (Tables S1 and S2). The PCR product was digested with NheI and XmaI (New England Biolabs) and cloned into

corresponding sites of pFB-MBP-MLH3-his (Ranjha et al., 2014). The preparation of other NBS1 variant expression constructs is described in Supplementary information. To prepare FLAG-NBS1-his, a *NBS1* sequence that was codon-optimized for expression in *Sf*9 cells (NBS1co) was purchased from Synbio Technologies and cloned into BamHI-XhoI sites of pFB-MBP-NBS1-his to create pFB-FLAG-NBS1co-his. To prepare pFB-MBP-MRE11-his, the MRE11 gene was amplified by PCR from pTP17 (a kind gift from Tanya Paull, University of Texas) using primers HMRE11-FO and HMRE11-RE (Tables S1 and S2). The amplified product was digested with NheI and XmaI, and cloned into the same sites in pFB-MBP-Sgs1-his plasmid (Cejka and Kowalczykowski, 2010)(the sequence of Sgs1 was removed during this step). The scheme and sequences of oligonucleotides used for cloning of the NBS1 fragments and all other constructs in this study are listed in Tables S1 and S2. Where indicated, 1.2 µg pCtIP was dephosphorylated in 20 µl reactions with 200 units of λ phosphatase (λ-PP, New England Biolabs) in 1x PMP buffer (New England Biolabs) supplemented with 1 mM magnesium chloride for 15 min at 30°C. For "mock" control, λ-PP was excluded from the reaction.

Nuclease assays

Unless indicated otherwise, nuclease assays (15 µl volume) were carried out in nuclease buffer containing 25 mM Tris-HCl pH 7.5, 5 mM magnesium acetate, 1 mM manganese acetate, 1 mM Dithiothreitol (DTT), 1 mM ATP, 0.25 mg/ml BSA (New England Biolabs), 1 mM phosphoenolpyruvate, 80 U/ml pyruvate kinase (Sigma), and 1 nM oligonucleotide-based DNA substrate (in molecules). The reactions were supplemented with 15 nM streptavidin (Sigma), and incubated for 5 min at room temperature to block the biotinylated end(s) of the DNA substrates. The recombinant proteins were then added to the reactions on ice and samples were incubated at 37°C for 30 min, unless indicated otherwise. Reactions were stopped by adding 0.5 µl ethylenediaminetetraacetic (0.5 M EDTA) and 1 µl Proteinase K (19 mg/ml, Roche), and incubated at 50°C for 30 min. Finally, 15 µl loading buffer (5% formamide, 20 mM EDTA, bromophenol blue) was added to all samples and the products were separated on 15% polyacrylamide denaturing urea gels (19:1 acrylamide-bisacrylamide, Bio-Rad), as described (Pinto et al., 2018). The gels were fixed in fixing solution (40% methanol, 10% acetic acid, 5% glycerol) for 30 min at room temperature and dried on a 3MM Chr paper (Whatman). The dried gels were exposed to storage phosphor screen (GE Healthcare) and scanned by a Typhoon Phosphor Imager (FLA 9500, GE Healthcare). Nuclease assays with circular ssDNA substrate (M13,

100 ng per reaction, New England Biolabs) were carried out similarly except the reaction buffer contained 60 mM NaCl and incubation time was extended to 2 h. The reaction products were separated on 1.1% agarose gels, which were stained with GelRed (1:20000, Biotium) after completion of electrophoresis for 45 min. The gels were imaged with gel imager (Ingenius^3, Syngene).

Preparation of oligonucleotide-based DNA substrates

All oligonucleotides were purified by polyacrylamide gel electrophoresis and purchased from Eurogentec. The labeling of oligonucleotides at the 5'-end was carried out by T4 polynucleotide kinase (New England Biolabs) and [γ-^{32}P] ATP (Perkin Elmer). The labeling of oligonucleotides at the 3'-end was carried out by terminal deoxynucleotidyl transferase (New England Biolabs) and [α-^{32}P] cordycepin 5' triphosphate, as described (Pinto et al., 2018). To prepare quadruple blocked 70-bp long DNA substrate, PC210 and PC211 oligonucleotides were used, as described previously (Cannavo and Cejka, 2014). To prepare single-blocked non-nicked substrate (Fig 7A), PC216C_5XSS (GA**T**GCATGAGGTGGAGTACGCGCCCGGGGAGCCCAAGGGCACGCCCTGGCACCCGCACCGCG GCA*C*T*T*A*C) was labeled at 5'-end and annealed with PC216_5XSS (GTAAGTGCCGCGGTGCGGGTGCCAGGGCGTGCCCTTGGGCTCCCCGGGCGCGTACTCCACCTC AT*G*C*A*T*C), the bold **T** represents the biotin modification and * represent phosphorothioate linkages between nucleotides. To prepare single blocked nicked substrate (Figs 7B and EV7D), PC216C_5XSS labeled at 5'-end was annealed with PC216_50nt (GTAAGTGCCGCGGTGCGGGTGCCAGGGCGTGCCCTTGGGCTCCCCGGGCG) and PC216_20nt_5XSS (CGTACTCCACCTCAT*G*C*A*T*C). To prepare substrate used in Fig EV7C, PC216C_5XSS labeled at 5'-end was annealed to PC216_20nt_5XSS.

Protein interaction assays

To test for interactions between recombinant proteins, the "bait" proteins were first immobilized on a resin (either M2 anti-FLAG affinity gel [Sigma] or Protein G agarose [Invitrogen] coupled to specific antibodies). The resin was then incubated with "prey" proteins in binding buffer, washed, and bound proteins were analyzed by western blotting. As a negative control, prey proteins were incubated with resin without bait proteins.

Specifically, to detect the interaction between pCtIP and NBS1 variants (Fig 2F and G), 1.5 µg anti-CtIP antibody (61141, Active Motif) was captured on 10 µl protein G beads

upon incubation in 150 µl PBS-T pH 7.4 (1.37 mM NaCl, 2.7 mM KCl, 10 mM Na_2HPO_4, 1.8 mM KH_2PO_4, 0.1% Tween 20) for 40 min at room temperature with continuous rotation. Next, 1 µg recombinant CtIP (mock-treated pCtIP or dephosphorylated λCtIP) was added and incubated in 60 µl binding buffer (25 mM Tris-HCl pH 7.5, 1 mM DTT, 3 mM EDTA, 50 mM NaCl, 0.2 mg/ml BSA) for 1 h at 4°C with continuous rotation. The resin with the immobilized antibody was washed 2 times with 150 µl wash buffer (25 mM Tris-HCl pH 7.5, 1 mM DTT, 3 mM EDTA, 80 mM NaCl, 0.05% Triton-X), and incubated with 320 nM NBS1 variants in 60 µl binding buffer for 1 h at 4° C with continuous rotation. The resin was then washed 3 times with 150 µl wash buffer. The proteins were eluted by incubation of the washed resin for 3 min at 95°C in 60 µl SDS buffer (50 mM Tris-HCl pH 6.8, 1.6% sodium dodecyl sulphate, 100 m DTT, 10% Glycerol, 0.01% bromophenol blue). CtIP and NBS1 variants were detected by western blot using anti-CtIP (61141, Active Motif, 1:1000) and anti-NBS1 (NB100-143, Novus Biologicals, 1:1000) antibodies. In assay shown in Fig 6C, 90 nM MRE11, MR or MRN was incubated with immobilized λCtIP or pCtIP as describe above. MRE11 was detected with anti-MRE11 antibody (ab214, Abcam, 1:1000).

To detect the interaction between MRE11-his and MBP-NBS1-his/MBP-NBS1 ΔMIR-his, or between MRE11-his and pCtIP/λCtIP as shown in Figs EV2 and 6A, respectively, 1.4 µg MRE11-his was immobilized on beads and coupled to anti-MRE11 antibody (ab214, Abcam). After washing, 200 nM MBP-NBS1-his/MBP-NBS1ΔMIR-his, or 330 nM pCtIP/λCtIP were incubated with the MRE11-coated resin in a 60 µl reaction in binding buffer as described above. For the assay shown in Fig EV2E, both MRE11-his and MBP-NBS1-his/MBP-NBS1 ΔMIR-his were detected by anti-his antibody (M091-3, MBL, 1:10000) by western blotting.

For the interaction assay shown in Fig 6B, 50 ml *Sf*9 cells were infected with RAD50-FLAG baculovirus. Cells were lysed and RAD50-FLAG (~300 ng) was immobilized on 30 µl anti-FLAG M2 affinity gel. Next, in a 150 µl reaction, 330 nM pCtIP/λCtIP was added and incubated in binding buffer for 1 h at 4°C with continuous rotation. Beads were washed 4 times with 300 µl wash buffer and proteins were eluted with wash buffer supplemented with 3X FLAG peptide (150 ng/µl, Sigma). Bound RAD50-FLAG was detected by western blotting using anti-FLAG antibodies (F3165, Sigma, 1:2000).

DR-GFP and SSA reporter assays

For DR-GFP HR repair reporter assay, DR-GFP U2OS cells (gift from Jeremy Stark) were plated at 20'000 cells/cm^2 in 6-well plates. After 24 h, cells were treansfected with control siRNA or siRNA against CtIP and NBS1, respectively. 48 h after siRNA transfection, cells were transfected with I-Sce1 expression plasmid (pCBASce). 4 h after transfection, the medium was replaced and a second transfection with siRNA aligos was carried out. 48 h after I-Sce1 transfection, cells were analyzed for GFP expression by flow cytometry on a LSRII Fortessa flow cytometer (BD).

Generation of siRNA-based NBS1 complementation system in U2OS cells

To generate the siRNA-based complementation system for NBS1, the Flp-In™ T-REx™ system (Thermo Fisher Scientific) was used according to the manufacturer's protocols. Briefly, myc-tagged full-length NBS1 cDNAs (wild type and mutants) were sub-cloned from retroviral expression constructs (Hari et al., 2010) and ligated into the pcDNA5/FRT/TO vector. Silent mutations were introduced in the siRNA target sequence (see below) by site-directed mutagenesis using the following mutagenesis primer (sense): 5'-GTTCAAAAACAGGAGGAAGACGTGAACGTTAGAAAAAGGCCAAGG-3'. A Flp-In T-REx U2OS cell line (gift from D. Durocher) was cultured in Dulbecco's modified Eagle medium (DMEM), supplemented with 10% fetal calf serum (FCS), 2 mM L-glutamine and penicillin-streptomycin antibiotics under standard cell culture conditions in a CO_2 incubator (37°C; 5% CO_2). NBS1-myc harboring vectors and the Flp-In recombinase expression plasmid pOG44 were mixed in a 1:9 ratio and transfected into the Flp-In T-REx U2OS cells. Stable clones were established by Hygromycin B (250 µg/ml) and Basticidin (10 µg/ml) selection and were characterized for inducible NBS1-myc expression by immunofluorescence and Western blotting.

Generation of the NBS1ΔN cell line

The NBS1ΔN cell line was generated according to a protocol published by the Zhang laboratory (Ran et al., 2013). The sgRNA target sequence (5'-GCGTTGAGTACGTTGTTGGA-3') was cloned into the PX330-U6-hSpCas9 vector and verified by sequencing. The targeting vector was then transfected into U2OS cells and clonal cell lines were isolated by dilution in 96-well plates. Single clones were analyzed for NBS1 expression by immunofluorescence. Several clones without detectable NBS1 expression were isolated and one of them was further characterized (data will be published elsewhere). Frame-shift inducing insertion/deletion (indel) mutations in all of the three NBS1 alleles present in U2OS cells were verified by Sanger sequencing of a PCR-amplified genomic fragment

that was cloned in the pCR II Blunt TOPO plasmid (sequences will be published elsewhere), indicating that the FHA BRCT domains coding region is essentially destroyed. Western blotting however revealed the presence of weakly expressed ~40 kDa protein that is recognized by a monoclonal antibody raised against full-length NBS1 (Genetex, clone 1D7, GTX70224) and is sensitive to downregulation of the NBS1 mRNA by siRNA transfection, thus suggesting that this cell line expresses low levels of hypomorphic C-terminal fragment of NBS1 that is produced by internal translation initiation within the NBS1 mRNA using an open reading frame generated by one of the indel mutations, similar to the NBS1 hypomorphic alleles expressed in cell lines derived from NBS patients (Maser et al., 2001).

In vivo resection assay

U2OS cell lines were grown on coverslips for 24 h prior to treatment. When indicated, cells were transfected with siRNAs against NBS1 (5'-GGAGGAAGAUGUCAAUGUUTT-dTdT-3') or CtIP (5'-GCUAAACAGGAACGAAUCTTdTdT-3') and incubated for 72 h. For heterologous expression of full-length recombinant myc-tagged NBS1, doxycyclin (1 μg/ml) was added 24 h prior to the experiment. For BrdU staining under native conditions, BrdU (10 μg/ml) was also added 24 h prior to the experiment. Cells were exposed to 5 Gy of IR and then incubated for 3 h at 37°C. The medium was removed, and cells were washed with PBS, followed by a brief pre-extraction on ice in CSK buffer (100 mM PIPES, pH 7.0; 100 mM NaCl; 300 mM Sucrose; 3 mM MgCl2; 0.4% Triton X-100). Cells were then fixed in 4% paraformaldehyde, washed and prepared for immunofluorescence analysis (see below).

Immunofluorescence

Cells were grown on glass coverslips and fixed with either ice-cold methanol for 10 minutes (for staining with NBS1 and MRE11 antibodies), or with 4% buffered formaldehyde (for staining with all other antibodies) for 15 min at room temperature, and subsequently permeabilized for 5 min in PBS containing 0.2% Triton X-100. Following 1h of blocking in blocking buffer (10% FBS, 3% BSA in PBS), primary antibody incubations were performed at room temperature for 2 h. Coverslips were washed three times with PBS and secondary antibody incubations were performed for 1h at room temperature in the dark. After washing with PBS for three times, coverslips were mounted on glass microscopy slides with Vectrashield mounting medium containing 0.5 μg/ml 4',6-diamidino-2-phenylindole dihydrochloride (DAPI). Widefiled image acquisition was done

on either a Leica DMI6000B inverted microscope equipped with a 63x Apochromat oil immersion objective (NA 1.3) using Leica's LAS-AF software or on a Zeiss AxioObserver Z1 widefield microscope, equipped with a Lumencor SpectraX illumination system and a 63x, 1.4-NA, i-plan apochromat oil-immersion objective, using Zeiss' ZEN (blue edition) software. Images were analyzed using Fiji software (Schindelin et al., 2012). Counting of BrdU foci or RPA2 foci was done with a Fiji macro written for automatic image analysis. The following antibodies were used at the indicated dilutions: rabbit anti NBS1 (Novus Biologicals, NB100-143, 1:500), affinity purified sheep anti MRE11 (Goldberg et al., 2003, 1:1000), mouse anti Myc (GeneTex, 9E10, GTX80249, 1:250), mouse anti BrdU (Amersham/GE healthcare, BU-1, RPN202, 1:100), mouse anti RPA2 (Abcam, 9H8, ab2175, 1:250).

Western blotting

SDS-PAGE and western blotting were performed using total extracts prepared from cultured cells following standard procedures. The following antibodies were used at the indicated dilutions: rabbit anti ATMpS1981 (Eptimics, YE070901r, 1:5000), rabbit anti ATM (Calbiochem, PC-116, 1:250), mouse anti CtIP (Santa Cruz, sc-271339, 1:250), mouse anti NBS1 (GeneTex, 1D7, GTX70224, 1:500), mouse anti RPA2 (Abcam, 9H8, ab2175, 1:500), rabbit anti SMC1 (Abcam, ab9262, 1:500), mouse anti RAD50 (GeneTex, 13B3, GTX70228, 1:1000), mouse anti MRE11 (Abcam, 12D7, ab214, 1:500), mouse anti Myc (GeneTex, 9E10, GTX80249, 1:250),, mouse anti Tubulin (Sigma, DM1A, T6199, 1:2000).

Clonogenic survival assay

U2OS FlpIn T-REx cell lines were transfected with siNBS1 for 48h and then plated at low density in medium supplemented with 0.5 µg/ml doxycycline. 24 h later, the plates were exposed to the indicated IR doses, followed by incubation for 12-14 days. Colonies were fixed and stained with Coomassie brilliant blue and the number of surviving colonies for each cell was counted. The percentage of surviving colonies for each cell line was calculated using the plating efficiencies of the non-irradiated cells as a reference. Survival experiments were carried out in biological triplicates.

Acknowledgements

We thank Dr. Jeremy Stark (City of Hope), Dr. Xiohua Wu (Scripps), Dr. Davide Moiani and Dr. John Tainer (MD Anderson Cancer Center), Dr. Tanya Paull (UT Austin) and Dan Durocher (Lunenfeld-Tanenbaum Research Insitute) for cell lines, plasmids and reagents. We thank members of the Cejka (add names) and Stucki laboratories for comments on the manuscript. This work was supported by the Swiss National Science Foundation grants 31003A_144284 to MS, 31003A_175444 to PC and European Research council grant 681630 to PC.

Author contributions

RA performed all biochemical experiments. SMH, AJ and DB performed cell biology experiments. All authors designed the experiments and analyzed the data. RA, PC and MS wrote the paper.

Conflict of interest

The authors declare that they have no conflict of interest

References

Anand, R., Pinto, C., and Cejka, P. (2018). Methods to Study DNA End Resection I: Recombinant Protein Purification. Methods Enzymol *600*, 25-66.

Anand, R., Ranjha, L., Cannavo, E., and Cejka, P. (2016). Phosphorylated CtIP Functions as a Co-factor of the MRE11-RAD50-NBS1 Endonuclease in DNA End Resection. Mol Cell *64*, 940-950.

Averbeck, N.B., Ringel, O., Herrlitz, M., Jakob, B., Durante, M., and Taucher-Scholz, G. (2014). DNA end resection is needed for the repair of complex lesions in G1-phase human cells. Cell Cycle *13*, 2509-2516.

Biehs, R., Steinlage, M., Barton, O., Juhasz, S., Kunzel, J., Spies, J., Shibata, A., Jeggo, P.A., and Lobrich, M. (2017). DNA Double-Strand Break Resection Occurs

during Non-homologous End Joining in G1 but Is Distinct from Resection during Homologous Recombination. Mol Cell *65*, 671-684 e675.
Cannavo, E., and Cejka, P. (2014). Sae2 promotes dsDNA endonuclease activity within Mre11-Rad50-Xrs2 to resect DNA breaks. Nature *514*, 122-125.
Cannavo, E., Johnson, D., Andres, S.N., Kissling, V.M., Reinert, J.K., Garcia, V., Erie, D.A., Hess, D., Thoma, N.H., Enchev, R.I.*, et al.* (2018). Regulatory control of DNA end resection by Sae2 phosphorylation. Nat Commun *9*, 4016.
Carney, J.P., Maser, R.S., Olivares, H., Davis, E.M., Le Beau, M., Yates, J.R., 3rd, Hays, L., Morgan, W.F., and Petrini, J.H. (1998). The hMre11/hRad50 protein complex and Nijmegen breakage syndrome: linkage of double-strand break repair to the cellular DNA damage response. Cell *93*, 477-486.
Cejka, P., and Kowalczykowski, S.C. (2010). The full-length Saccharomyces cerevisiae Sgs1 protein is a vigorous DNA helicase that preferentially unwinds holliday junctions. J Biol Chem *285*, 8290-8301.
Cerosaletti, K.M., and Concannon, P. (2003). Nibrin forkhead-associated domain and breast cancer C-terminal domain are both required for nuclear focus formation and phosphorylation. J Biol Chem *278*, 21944-21951.
Chen, L., Nievera, C.J., Lee, A.Y., and Wu, X. (2008). Cell cycle-dependent complex formation of BRCA1.CtIP.MRN is important for DNA double-strand break repair. J Biol Chem *283*, 7713-7720.
Chen, L., Trujillo, K.M., Van Komen, S., Roh, D.H., Krejci, L., Lewis, L.K., Resnick, M.A., Sung, P., and Tomkinson, A.E. (2005). Effect of amino acid substitutions in the rad50 ATP binding domain on DNA double strand break repair in yeast. J Biol Chem *280*, 2620-2627.
Connelly, J.C., de Leau, E.S., and Leach, D.R. (2003). Nucleolytic processing of a protein-bound DNA end by the E. coli SbcCD (MR) complex. DNA Repair (Amst) *2*, 795-807.
de Jager, M., van Noort, J., van Gent, D.C., Dekker, C., Kanaar, R., and Wyman, C. (2001). Human Rad50/Mre11 is a flexible complex that can tether DNA ends. Mol Cell *8*, 1129-1135.
Deng, S.K., Gibb, B., de Almeida, M.J., Greene, E.C., and Symington, L.S. (2014). RPA antagonizes microhomology-mediated repair of DNA double-strand breaks. Nat Struct Mol Biol *21*, 405-412.
Desai-Mehta, A., Cerosaletti, K.M., and Concannon, P. (2001). Distinct functional domains of nibrin mediate Mre11 binding, focus formation, and nuclear localization. Mol Cell Biol *21*, 2184-2191.
Deshpande, R.A., Lee, J.H., Arora, S., and Paull, T.T. (2016). Nbs1 Converts the Human Mre11/Rad50 Nuclease Complex into an Endo/Exonuclease Machine Specific for Protein-DNA Adducts. Mol Cell *64*, 593-606.
Deshpande, R.A., Williams, G.J., Limbo, O., Williams, R.S., Kuhnlein, J., Lee, J.H., Classen, S., Guenther, G., Russell, P., Tainer, J.A.*, et al.* (2014). ATP-driven Rad50 conformations regulate DNA tethering, end resection, and ATM checkpoint signaling. EMBO J *33*, 482-500.
Dutta, A., Eckelmann, B., Adhikari, S., Ahmed, K.M., Sengupta, S., Pandey, A., Hegde, P.M., Tsai, M.S., Tainer, J.A., Weinfeld, M.*, et al.* (2017). Microhomology-mediated end joining is activated in irradiated human cells due to phosphorylation-dependent formation of the XRCC1 repair complex. Nucleic Acids Res *45*, 2585-2599.

Falck, J., Coates, J., and Jackson, S.P. (2005). Conserved modes of recruitment of ATM, ATR and DNA-PKcs to sites of DNA damage. Nature *434*, 605-611.
Feng, W., and Jasin, M. (2017). BRCA2 suppresses replication stress-induced mitotic and G1 abnormalities through homologous recombination. Nat Commun *8*, 525.
Garcia, V., Phelps, S.E., Gray, S., and Neale, M.J. (2011). Bidirectional resection of DNA double-strand breaks by Mre11 and Exo1. Nature *479*, 241-244.
Goldberg, M., Stucki, M., Falck, J., D'Amours, D., Rahman, D., Pappin, D., Bartek, J., and Jackson, S.P. (2003). MDC1 is required for the intra-S-phase DNA damage checkpoint. Nature *421*, 952-956.
Gravel, S., Chapman, J.R., Magill, C., and Jackson, S.P. (2008). DNA helicases Sgs1 and BLM promote DNA double-strand break resection. Genes Dev *22*, 2767-2772.
Hari, F.J., Spycher, C., Jungmichel, S., Pavic, L., and Stucki, M. (2010). A divalent FHA/BRCT-binding mechanism couples the MRE11-RAD50-NBS1 complex to damaged chromatin. EMBO Rep *11*, 387-392.
Huertas, P., Cortes-Ledesma, F., Sartori, A.A., Aguilera, A., and Jackson, S.P. (2008). CDK targets Sae2 to control DNA-end resection and homologous recombination. Nature *455*, 689-692.
Huertas, P., and Jackson, S.P. (2009). Human CtIP mediates cell cycle control of DNA end resection and double strand break repair. J Biol Chem *284*, 9558-9565.
Keeney, S., and Kleckner, N. (1995). Covalent protein-DNA complexes at the 5' strand termini of meiosis-specific double-strand breaks in yeast. Proceedings of the National Academy of Sciences of the United States of America *92*, 11274-11278.
Kim, J.H., Grosbart, M., Anand, R., Wyman, C., Cejka, P., and Petrini, J.H. (2017). The Mre11-Nbs1 Interface Is Essential for Viability and Tumor Suppression. Cell Rep *18*, 496-507.
Lafrance-Vanasse, J., Williams, G.J., and Tainer, J.A. (2015). Envisioning the dynamics and flexibility of Mre11-Rad50-Nbs1 complex to decipher its roles in DNA replication and repair. Prog Biophys Mol Biol *117*, 182-193.
Lee, J.H., and Paull, T.T. (2005). ATM activation by DNA double-strand breaks through the Mre11-Rad50-Nbs1 complex. Science *308*, 551-554.
Lemacon, D., Jackson, J., Quinet, A., Brickner, J.R., Li, S., Yazinski, S., You, Z., Ira, G., Zou, L., Mosammaparast, N.*, et al.* (2017). MRE11 and EXO1 nucleases degrade reversed forks and elicit MUS81-dependent fork rescue in BRCA2-deficient cells. Nat Commun *8*, 860.
Liang, J., Suhandynata, R.T., and Zhou, H. (2015). Phosphorylation of Sae2 Mediates Forkhead-associated (FHA) Domain-specific Interaction and Regulates Its DNA Repair Function. The Journal of biological chemistry *290*, 10751-10763.
Limbo, O., Yamada, Y., and Russell, P. (2018). Mre11-Rad50-dependent activity of ATM/Tel1 at DNA breaks and telomeres in the absence of Nbs1. Mol Biol Cell *29*, 1389-1399.
Lloyd, J., Chapman, J.R., Clapperton, J.A., Haire, L.F., Hartsuiker, E., Li, J., Carr, A.M., Jackson, S.P., and Smerdon, S.J. (2009). A supramodular FHA/BRCT-repeat architecture mediates Nbs1 adaptor function in response to DNA damage. Cell *139*, 100-111.

Ma, J.L., Kim, E.M., Haber, J.E., and Lee, S.E. (2003). Yeast Mre11 and Rad1 proteins define a Ku-independent mechanism to repair double-strand breaks lacking overlapping end sequences. Mol Cell Biol *23*, 8820-8828.
Mijic, S., Zellweger, R., Chappidi, N., Berti, M., Jacobs, K., Mutreja, K., Ursich, S., Ray Chaudhuri, A., Nussenzweig, A., Janscak, P.*, et al.* (2017). Replication fork reversal triggers fork degradation in BRCA2-defective cells. Nat Commun *8*, 859.
Mimitou, E.P., and Symington, L.S. (2008). Sae2, Exo1 and Sgs1 collaborate in DNA double-strand break processing. Nature *455*, 770-774.
Moore, J.K., and Haber, J.E. (1996). Cell cycle and genetic requirements of two pathways of nonhomologous end-joining repair of double-strand breaks in Saccharomyces cerevisiae. Mol Cell Biol *16*, 2164-2173.
Nakada, D., Matsumoto, K., and Sugimoto, K. (2003). ATM-related Tel1 associates with double-strand breaks through an Xrs2-dependent mechanism. Genes Dev *17*, 1957-1962.
Neale, M.J., Pan, J., and Keeney, S. (2005). Endonucleolytic processing of covalent protein-linked DNA double-strand breaks. Nature *436*, 1053-1057.
Nimonkar, A.V., Genschel, J., Kinoshita, E., Polaczek, P., Campbell, J.L., Wyman, C., Modrich, P., and Kowalczykowski, S.C. (2011). BLM-DNA2-RPA-MRN and EXO1-BLM-RPA-MRN constitute two DNA end resection machineries for human DNA break repair. Genes Dev *25*, 350-362.
Oh, J., Al-Zain, A., Cannavo, E., Cejka, P., and Symington, L.S. (2016). Xrs2 Dependent and Independent Functions of the Mre11-Rad50 Complex. Mol Cell *64*, 405-415.
Paull, T.T. (2010). Making the best of the loose ends: Mre11/Rad50 complexes and Sae2 promote DNA double-strand break resection. DNA Repair (Amst) *9*, 1283-1291.
Paull, T.T., and Gellert, M. (1998). The 3' to 5' exonuclease activity of Mre 11 facilitates repair of DNA double-strand breaks. Mol Cell *1*, 969-979.
Paull, T.T., and Gellert, M. (1999). Nbs1 potentiates ATP-driven DNA unwinding and endonuclease cleavage by the Mre11/Rad50 complex. Genes Dev *13*, 1276-1288.
Pinto, C., Anand, R., and Cejka, P. (2018). Methods to Study DNA End Resection II: Biochemical Reconstitution Assays. Methods Enzymol *600*, 67-106.
Rahal, E.A., Henricksen, L.A., Li, Y., Williams, R.S., Tainer, J.A., and Dixon, K. (2010). ATM regulates Mre11-dependent DNA end-degradation and microhomology-mediated end joining. Cell Cycle *9*, 2866-2877.
Ranjha, L., Anand, R., and Cejka, P. (2014). The Saccharomyces cerevisiae Mlh1-Mlh3 heterodimer is an endonuclease that preferentially binds to Holliday junctions. J Biol Chem *289*, 5674-5686.
Ranjha, L., Howard, S.M., and Cejka, P. (2018). Main steps in DNA double-strand break repair: an introduction to homologous recombination and related processes. Chromosoma.
Rass, E., Grabarz, A., Plo, I., Gautier, J., Bertrand, P., and Lopez, B.S. (2009). Role of Mre11 in chromosomal nonhomologous end joining in mammalian cells. Nat Struct Mol Biol *16*, 819-824.
Ray Chaudhuri, A., Callen, E., Ding, X., Gogola, E., Duarte, A.A., Lee, J.E., Wong, N., Lafarga, V., Calvo, J.A., Panzarino, N.J.*, et al.* (2016). Replication fork stability confers chemoresistance in BRCA-deficient cells. Nature *535*, 382-387.

Reginato, G., Cannavo, E., and Cejka, P. (2018). Physiological protein blocks direct the Mre11-Rad50-Xrs2 and Sae2 nuclease complex to initiate DNA end resection. Genes Dev.
Sartori, A.A., Lukas, C., Coates, J., Mistrik, M., Fu, S., Bartek, J., Baer, R., Lukas, J., and Jackson, S.P. (2007). Human CtIP promotes DNA end resection. Nature *450*, 509-514.
Schiller, C.B., Lammens, K., Guerini, I., Coordes, B., Feldmann, H., Schlauderer, F., Mockel, C., Schele, A., Strasser, K., Jackson, S.P.*, et al.* (2012). Structure of Mre11-Nbs1 complex yields insights into ataxia-telangiectasia-like disease mutations and DNA damage signaling. Nat Struct Mol Biol *19*, 693-700.
Schlacher, K., Christ, N., Siaud, N., Egashira, A., Wu, H., and Jasin, M. (2011). Double-strand break repair-independent role for BRCA2 in blocking stalled replication fork degradation by MRE11. Cell *145*, 529-542.
Sharma, S., Javadekar, S.M., Pandey, M., Srivastava, M., Kumari, R., and Raghavan, S.C. (2015). Homology and enzymatic requirements of microhomology-dependent alternative end joining. Cell Death Dis *6*, e1697.
Shibata, A., Moiani, D., Arvai, A.S., Perry, J., Harding, S.M., Genois, M.M., Maity, R., van Rossum-Fikkert, S., Kertokalio, A., Romoli, F.*, et al.* (2014). DNA double-strand break repair pathway choice is directed by distinct MRE11 nuclease activities. Mol Cell *53*, 7-18.
Spycher, C., Miller, E.S., Townsend, K., Pavic, L., Morrice, N.A., Janscak, P., Stewart, G.S., and Stucki, M. (2008). Constitutive phosphorylation of MDC1 physically links the MRE11-RAD50-NBS1 complex to damaged chromatin. J Cell Biol *181*, 227-240.
Stark, J.M., Pierce, A.J., Oh, J., Pastink, A., and Jasin, M. (2004). Genetic steps of mammalian homologous repair with distinct mutagenic consequences. Mol Cell Biol *24*, 9305-9316.
Stewart, G.S., Maser, R.S., Stankovic, T., Bressan, D.A., Kaplan, M.I., Jaspers, N.G., Raams, A., Byrd, P.J., Petrini, J.H., and Taylor, A.M. (1999). The DNA double-strand break repair gene hMRE11 is mutated in individuals with an ataxia-telangiectasia-like disorder. Cell *99*, 577-587.
Stracker, T.H., and Petrini, J.H. (2011). The MRE11 complex: starting from the ends. Nat Rev Mol Cell Biol *12*, 90-103.
Taylor, E.M., Cecillon, S.M., Bonis, A., Chapman, J.R., Povirk, L.F., and Lindsay, H.D. (2010). The Mre11/Rad50/Nbs1 complex functions in resection-based DNA end joining in Xenopus laevis. Nucleic Acids Res *38*, 441-454.
Trujillo, K.M., Yuan, S.S., Lee, E.Y., and Sung, P. (1998). Nuclease activities in a complex of human recombination and DNA repair factors Rad50, Mre11, and p95. J Biol Chem *273*, 21447-21450.
Truong, L.N., Li, Y., Shi, L.Z., Hwang, P.Y., He, J., Wang, H., Razavian, N., Berns, M.W., and Wu, X. (2013). Microhomology-mediated End Joining and Homologous Recombination share the initial end resection step to repair DNA double-strand breaks in mammalian cells. Proc Natl Acad Sci U S A *110*, 7720-7725.
Tsukamoto, Y., Mitsuoka, C., Terasawa, M., Ogawa, H., and Ogawa, T. (2005). Xrs2p regulates Mre11p translocation to the nucleus and plays a role in telomere elongation and meiotic recombination. Mol Biol Cell *16*, 597-608.
Usui, T., Ogawa, H., and Petrini, J.H. (2001). A DNA damage response pathway controlled by Tel1 and the Mre11 complex. Mol Cell *7*, 1255-1266.

Wang, H., Shi, L.Z., Wong, C.C., Han, X., Hwang, P.Y., Truong, L.N., Zhu, Q., Shao, Z., Chen, D.J., Berns, M.W*., et al.* (2013). The interaction of CtIP and Nbs1 connects CDK and ATM to regulate HR-mediated double-strand break repair. PLoS Genet *9*, e1003277.
Wang, W., Daley, J.M., Kwon, Y., Krasner, D.S., and Sung, P. (2017). Plasticity of the Mre11-Rad50-Xrs2-Sae2 nuclease ensemble in the processing of DNA-bound obstacles. Genes Dev *31*, 2331-2336.
Wang, Y., Cortez, D., Yazdi, P., Neff, N., Elledge, S.J., and Qin, J. (2000). BASC, a super complex of BRCA1-associated proteins involved in the recognition and repair of aberrant DNA structures. Genes Dev *14*, 927-939.
Williams, R.S., Dodson, G.E., Limbo, O., Yamada, Y., Williams, J.S., Guenther, G., Classen, S., Glover, J.N., Iwasaki, H., Russell, P*., et al.* (2009). Nbs1 flexibly tethers Ctp1 and Mre11-Rad50 to coordinate DNA double-strand break processing and repair. Cell *139*, 87-99.
Williams, R.S., Moncalian, G., Williams, J.S., Yamada, Y., Limbo, O., Shin, D.S., Groocock, L.M., Cahill, D., Hitomi, C., Guenther, G*., et al.* (2008). Mre11 dimers coordinate DNA end bridging and nuclease processing in double-strand-break repair. Cell *135*, 97-109.
You, Z., Chahwan, C., Bailis, J., Hunter, T., and Russell, P. (2005). ATM activation and its recruitment to damaged DNA require binding to the C terminus of Nbs1. Mol Cell Biol *25*, 5363-5379.
Yu, X., and Chen, J. (2004). DNA damage-induced cell cycle checkpoint control requires CtIP, a phosphorylation-dependent binding partner of BRCA1 C-terminal domains. Molecular and cellular biology *24*, 9478-9486.
Yuan, J., and Chen, J. (2009). N terminus of CtIP is critical for homologous recombination-mediated double-strand break repair. J Biol Chem *284*, 31746-31752.
Zhou, H., Kawamura, K., Yanagihara, H., Kobayashi, J., and Zhang-Akiyama, Q.M. (2017). NBS1 is regulated by two kind of mechanisms: ATM-dependent complex formation with MRE11 and RAD50, and cell cycle-dependent degradation of protein. J Radiat Res *58*, 487-494.
Zhu, X.D., Kuster, B., Mann, M., Petrini, J.H., and de Lange, T. (2000). Cell-cycle-regulated association of RAD50/MRE11/NBS1 with TRF2 and human telomeres. Nat Genet *25*, 347-352.
Zhu, Z., Chung, W.H., Shim, E.Y., Lee, S.E., and Ira, G. (2008). Sgs1 helicase and two nucleases Dna2 and Exo1 resect DNA double-strand break ends. Cell *134*, 981-994.

Figure Legends

Figure 1 - NBS1 in *trans* with MR and pCtIP cleaves DNA similarly as MRN-pCtIP.

A A representative 10% polyacrylamide gel showing purification of recombinant MBP-NBS1-his. The gel was stained with Coomassie brilliant blue. Amylose flowthrough and eluate, flowthrough and eluate from amylose resin; Ni-NTA flowthrough and eluate,

flowthrough and eluate from nickel-nitrilotriacetic acid (Ni-NTA). * indicates truncated products.

B Nuclease assay with MR, MBP-NBS1-his (denoted here and thereafter NBS1 for brevity), MRN and pCtIP on 3'-end labeled 70-bp dsDNA with all ends blocked with streptavidin. Samples were separated on 15 % denaturing polyacrylamide gel. S, streptavidin; red asterisk, position of the ^{32}P-label.

C Nuclease assay as in (B) but with 5'-end labeled 70-bp dsDNA.

Figure 2 - FHA and BRCT domains of NBS1 are important for MR-pCtIP stimulation while MRE11-NBS1 interaction is essential.

A A schematic representation of purified recombinant wild type NBS1 and variants. All constructs were MBP tagged at the N- and his-tagged at the C-terminus.

B A representative polyacrylamide gel (4-15%) stained with Coomassie brilliant blue showing purified NBS1 variants. All constructs were MBP tagged at the N- and his-tagged at the C-terminus.

C A representative nuclease assay with MR, pCtIP and various concentrations of MBP-NBS1-his (labeled NBS1) on 3'-end labeled dsDNA.

D Quantitation of experiments such as shown in (C). Averages shown; n = 5; error bars, SEM.

E The effect of NBS1 variants containing MRE11 interaction region (MIR) on the nuclease of MR and pCtIP. Quantitation of experiments such as shown in Fig EV2A. Averages shown; n ≥ 4, error bars, SEM. Statistical significance denotations represent the analysis between wild type full-length NBS1 (in black) and the corresponding concentrations of the NBS1 variants; ns ($p > 0.05$, not significant), * ($p < 0.05$), ** ($p < 0.01$), *** ($p < 0.001$), two-tailed *t*-test.

F Analysis of pCtIP binding to NBS1 variants. Anti-CtIP antibody was immobilized on Protein G agarose, bound to pCtIP, and tested for interactions with the indicated NBS1 variants (see cartoon at the top). Western blot of eluates (left part) was performed with anti-CtIP and anti-NBS1 antibodies. Right part (input) indicates that the anti-NBS1 antibody recognizes the NBS1 constructs to a similar level.

G Analysis of phosphorylated (pCtIP, mock-treated) or λ phosphatase treated (λCtIP) interactions with NBS1. The CtIP variants were immobilized on protein G

agarose, and incubated with NBS1 (see cartoon at the top). The western blot was performed with anti-CtIP and anti-NBS1 antibodies.

H The effect of NBS1 variants containing or lacking MRE11 interaction region (MIR) on the nuclease of MR and pCtIP. Quantitation of experiments such as shown in Fig EV2A and B. Averages shown, n ≥ 3, error bars, SEM. The quantitation of wild type NBS1 (NBS1 WT, in black) is the same as in panel (E) and is shown again for reference.

Figure 3 - Without pCtIP, NBS1 promotes the MR endonuclease independently of its FHA and BRCT domains.

A Nuclease assays with MR and various NBS1 fragments on oligonucleotide-based 5'-end labeled dsDNA. The reaction buffer contained 60 mM NaCl and reactions were incubated for 2 h.

B Quantitation of experiments such as shown in (A). Averages shown; n ≥ 3, error bars, SEM.

C Nuclease assays with MR and various NBS1 fragments on M13 ssDNA. The reaction products were separated on agarose gels (1.1%). The reaction buffer contained 60 mM NaCl and reactions were incubated for 2 h.

D Quantitation of experiments such as shown in (C). Averages shown; n = 3, error bars, SEM.

Figure 4 - The function of NBS1 in DNA end resection *in vivo*.

A A schematic representation of the NBS1 knockdown-rescue experiments in U2OS cells.

B Immunofuorescence experiment showing efficient depletion of NBS1 by siRNA and cytoplasmic localization of MRE11 in the NBS1-depleted cells. Experssion of myc-tagged recombinant NBS1 restores MRE11 nuclear localization.

C Western blot showing efficient depletion of NBS1 and CtIP by siRNA treansfection and expression of siRNA-resistant myc-tagged recombinant NBS1.

D In vivo resection assay using BrdU staining under native conditions to directly detect ssDNA at sites of DSBs

E In vivo resection assay using RPA2 staining as a marker for ssDNA present at sites of DSBs

F Quantification of the experiment shown in D. At least 100 cells were assessed per condition

G Quantification of the experiment shown in C. At least 100 cells were assessed per condition

H Quantification of resection activity in NBS1ΔN cells complemented with wild type (WT) or R28A K160M mutant (DM) NBS1 and either mock depleted (siCtrl) or depleted of CtIP (siCtIP). At least 300 cells were assessed per condition. Statistical significance was determined using ordinary one-way ANOVA with Tukey's multiple comparison test.

I Quantitation of the single strand annealing (SSA) reporter assay in U2OS cells. All cells were treated with DMSO; where indicated, both PFM03 (50 μM) and PFM39 (50 μM) MRE11 inhibitors were added, diluted in DMSO. Averages shown; n = 4, error bars, SEM.

Figure 5 - Phosphorylation of CtIP is partially dispensable for MR stimulation in the absence of NBS1.

A Nuclease assays with MR and pCtIP on 3'-end labeled dsDNA, incubated for 2 h.

B Quantitation of experiments such as shown in (A). Averages shown; n = 2; error bars, range.

C Nuclease assays with MRN, MR and various concentrations of pCtIP (mock-treated) or λCtIP on 5'-end labeled dsDNA, incubated for 2 h.

D Quantitation of experiments such as shown in (C). Averages shown; n = 3; error bars, SEM.

E Phosphorylated CtIP was mock-incubated (pCtIP, lane 2) or treated with λ phosphatase (λCtIP, lane 3). The proteins were separated on a 10% polyacrylamide gel and stained with Coomassie brilliant blue.

F Quantitation of kinetic nuclease assays with MRN and pCtIP (mock-treated) or λCtIP. Averages shown; n = 3; error bars; SEM. Statistical denotations, ** ($p < 0.01$), two-tailed *t*-test.

G Quantitation of nuclease assays as in (E), but with MR complex instead of MRN. Averages shown; n = 3; error bars, SEM. Statistical denotations, ns ($p > 0.05$), two-tailed *t*-test.

H Nuclease assays with MR, MRN, pCtIP or pCtIP T847A, as indicated, on 5'-end labeled dsDNA. Reactions were incubated for 2 h.

I Quantitation of experiments such as shown in (G). Averages shown; n = 4; error bars, SEM.

Figure 6 - CtIP phosphorylation is dispensable for its interaction with MRE11 and RAD50.

A Interaction between MRE11 and CtIP. MRE11 was immobilized on antibody-coupled Protein G agarose, and incubated with pCtIP or λCtIP (see cartoon). Western blot analysis of bound proteins was performed with anti-MRE11 and anti-CtIP antibodies.

B Interaction between RAD50 and CtIP. RAD50-FLAG was immobilized on anti-FLAG affinity resin and incubated with pCtIP and λCtIP (see cartoon). Western blot analysis of bound proteins was performed with anti-FLAG and anti-CtIP antibodies.

C Interaction between MRE11, MR or MRN and pCtIP or λCtIP, as indicated. Phosphorylated (pCtIP) or λ phosphatase-treated CtIP (λCtIP) were immobilized on antibody-coupled Protein G agarose, and incubated with MRE11, MR or MRN complexes (see cartoon). Bound proteins were analyzed by western blot using anti-CtIP and anti-MRE11 antibodies.

Figure 7 - NBS1 promotes the access of the MRN complex to dsDNA to promote DNA cleavage.

A Representative nuclease assays with MRE11, MR, MRN and pCtIP, as indicated, on 5'-end labeled dsDNA with single streptavidin-blocked end (S). The substrate contained 5 phosphorothioate bonds (PTO) at both 3'-ends to prevent exonucleolytic DNA degradation. Reactions were incubated for 2 h.

B Representative nuclease assays as in (A), but with a substrate containing a nick in the top oligonucleotide (20 nt away from the 3'-end, see cartoon).

C Quantitation of experiments such as shown in (A). Averages shown; n ≥ 4; error bars, SEM.

D Quantitation of experiments such as shown in (B). Averages shown; n = 3; error bars, SEM.

E Quantitation of experiments such as shown in (B). Averages shown; n = 3; error bars, SEM.

Figure 8 - A model for MRN and CtIP functions in endonucleolytic DNA cleavage.

A When phosphorylated CtIP and MRN are present (in S-G2), CtIP phosphorylation is detected by the FHA and BRCT domains of NBS1 (1), which in turn promotes DNA cleavage by MR via direct interaction with MRE11, mediated by the MRE11-interaction region of NBS1 (2). This results in maximal DNA end resection activity compatible with homologous recombination.

B In the absence of NBS1 function (see text), CtIP promotes the nuclease of MR in a reaction that is partly independent of its phosphorylation (3). This results in low resection activity of MR, which may be sufficient for resection in G1 required for MMEJ.

C In the absence of CtIP, NBS1, through its MRE11-interaction region, but independently of its FHA and BRCT domains, promotes the MR endonuclease (4). This activity is likely very limited and therefore unlikely to be physiologically relevant.

Expanded View Figure Legends

Expanded View figure 1 (related to figure 1)

A Samples from a representative purification of the MR complex were analyzed by 10% polyacrylamide gel electrophoresis. The gel was stained with Coomassie brilliant blue. FLAG flowthrough and eluate, flowthrough and eluate from anti-FLAG affinity resin.

B Samples from a representative purification of the MRN complex analyzed by 10% polyacrylamide gel electrophoresis.

C Samples from a representative purification of phosphorylated CtIP (expressed and purified with phosphatase inhibitors) analyzed by 10% polyacrylamide gel electrophoresis.

D Polyacrylamide gel stained with Coomassie brilliant blue showing the partial cleavage of MBP-NBS1-his by PreScission protease (PP). The PP recognition site is in between the MBP tag and NBS1. 2 μg recombinant MBP-NBS1-his was incubated for 1 h at 4°C with 1 μg of PreScission protease.

E Nuclease assays with MR and pCtIP and either uncleaved (left panel) and partially cleaved MBP-NBS1 (right panel, ~50% cleaved) with PreScission protease. 5'-end labeled dsDNA was used as a substrate.

F Polyacrylamide gel stained with Coomassie brilliant showing purified recombinant MBP-NBS1-his and FLAG-NBS1-his. * indicates truncated product.

G Nuclease assays with MR and pCtIP and either MBP-NBS1-his (left panel) or FLAG-NBS1 (right panel). 3'-end labeled dsDNA was used a substrate.

Expanded View figure 2 (related to figure 2)

A Representative nuclease assays with MR, pCtIP and various MBP-NBS1-his fragments containing MRE11-interaction region (MIR), using 3'-end labeled dsDNA as a substrate.

B Representative nuclease assays with MR, pCtIP and various NBS1 fragments lacking MRE11-interaction region (MIR) on 3'-end labeled dsDNA.

C Representative nuclease assays with MR, pCtIP and various concentrations of MBP-NBS1ΔMIR, using 3'-end labeled dsDNA as a substrate.

D A representative 10% polyacrylamide gel stained with Coomassie brilliant blue showing purified recombinant MRE11-his.

E Interaction of MRE11 with NBS1. MRE11 was immobilized on antibody-coupled Protein G agarose, and incubated with MBP-NBS1-his or MBP-NBS1ΔMIR-his (see cartoon). Bound proteins were analyzed by western blot with anti-his antibodies.

Expanded View figure 3 (related to figure 3)

A Nuclease assay with various NBS1 fragments (all MBP tagged at the N-terminus and his-tagged at the C-terminus) without MR and pCtIP, using 5'-end labeled dsDNA as a substrate. The reaction buffer contained 60 mM NaCl and reactions were incubated for 2 h.

B Nuclease assay with MR and MBP-NBS1-his (denoted NBS1), with and without ATP on 5'-end labeled dsDNA. The reaction buffer contained 60 mM NaCl and reactions were incubated for 2 h. The DNA cleavage reaction requires ATP, in agreement with observations that ATPase-deficient RAD50 mutants are incapable of resection *in vivo*.

C Quantitation of experiments such as shown in (B). Averages shown, n = 2, error bars, range.

D Nuclease assays with MR and MBP-NBS1-his (denoted NBS1), with and without ATP, using M13 ssDNA as a substrate. The reaction buffer contained 60 mM NaCl and reactions were incubated for 2 h. The reactions were separated on 1.1% agarose gel. ATP only moderately stimulated M13 ssDNA cleavage.

E Quantitation of experiments such as shown in (D). Averages shown; n = 2, error bars, range.

F Nuclease assay with MR and MBP-NBS1 as in panel (D), but with or without RPA. RPA inhibits M13 ssDNA cleavage (this panel) and ATP is partially dispensable (see panels D and E). In cells, RPA is ubiquitous and RAD50 ATPase-deficient mutants are incapable of resection. Therefore, we believe that the M13-based assays do not accurately mimic the reaction occurring *in vivo*, and that the clipping of dsDNA (see panels B and C) is a better model.

Expanded View figure 4 (related to figure 4)

A Western blot of FlpIn T-REx NBS1-myc expressing cells. Expression of recombinant NBS1 was induced for 24 h with doxycycline (DOX) prior to extract preparation

B Clonogenic survival assay showing that expression of siRNA-resistant recombinant NBS1 rescues radiosensitivity of NBS1-depleted cells

C Western blot showing efficient downregulation of CtIP and NBS1 in the HR reporter assay in D

D HR repair reporter assay after CtIP and NBS1 depletion. Bars and error bars represent mean and SD of 4 independent experiments. Statistical significance was tested by unpaired t-test (p=0.0242).

E Quantification of resection activity in wild type U2OS cells and NBS1ΔN cells. At least 260 cells were assessed per condition.

F Western blot of extracts prepared from wild type U2OS cells, NBS1ΔN cells and NBS1ΔN cells stably expressing mNeonGreen (mNG) tagged wild type (WT) and R28A K160M mutant (DM) full-length NBS1, either mock-depleted (siCtrl) or depleted of CtIP (siCtIP) by siRNA. Note the presence of a presumably hypomorphic 40 kDa C-terminal fragment of NBS1 ($NBS1^{hm}$) in the NBS1ΔN cell line.

G Immunofluorescence of NBS1ΔN U2OS cells stably expressing mNeonGreen (mNG) tagged wild type (WT) and R28A K160M mutant (DM) full-length NBS1. Note that MRE11 nuclear localization is partially impaired in NBS1ΔN cells, which is fully rescued by heterologous expression of NBS1.

Expanded View figure 5 (related to figure 5)

A Representative nuclease assays with MR, MRN and pCtIP or λCtIP using 5'-end labeled dsDNA. Quantitations of these and similar experiments is shown in Fig 5F and G. Reactions were incubated for 2 h.

B Nuclease assays with MR and pCtIP T847A or λCtIP T847A on 5'-end labeled dsDNA. Reactions were incubated for 2 h.

C Quantitation of experiments such as shown in (E). Averages shown; n = 2; error bars, range.

Expanded View figure 7 (related to figure 7)

A Nuclease assays with MRN and pCtIP and various concentrations of MRE11 inhibitor PFM03 (endonuclease inhibitor) on 5'-end labeled dsDNA.

B Nuclease assays with MRN and pCtIP and various concentrations of MRE11 inhibitor PFM39 (exonuclease inhibitor) on 5'-end labeled dsDNA.

C Nuclease assays as in Fig 7B, but with a substrate missing the top left oligonucleotide.

D Nuclease assays as in Fig 7B, but with a substrate that was not blocked with streptavidin.

Figure 1

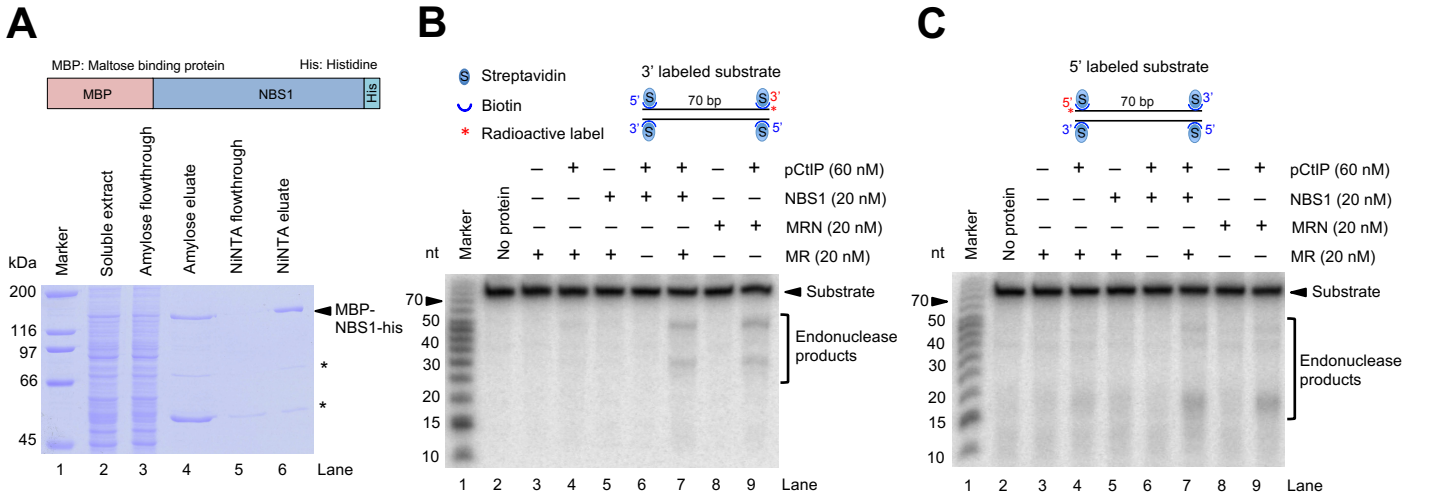
A
MBP: Maltose binding protein
His: Histidine
MBP
NBS1
His
kDa
Marker
Soluble extract
Amylose flowthrough
Amylose eluate
NiNTA flowthrough
NiNTA eluate
200
116
97
66
45
MBP-NBS1-his
*
*
1 2 3 4 5 6 Lane
B
Streptavidin
Biotin
Radioactive label
3' labeled substrate
5'
70 bp
3'
3'
5'
pCtIP (60 nM)
NBS1 (20 nM)
MRN (20 nM)
MR (20 nM)
nt
Marker
No protein
70
50
40
30
20
15
10
Substrate
Endonuclease products
1 2 3 4 5 6 7 8 9 Lane
C
5' labeled substrate
5'
70 bp
3'
3'
5'
pCtIP (60 nM)
NBS1 (20 nM)
MRN (20 nM)
MR (20 nM)
nt
Marker
No protein
70
50
40
30
20
15
10
Substrate
Endonuclease products
1 2 3 4 5 6 7 8 9 Lane

Figure 2

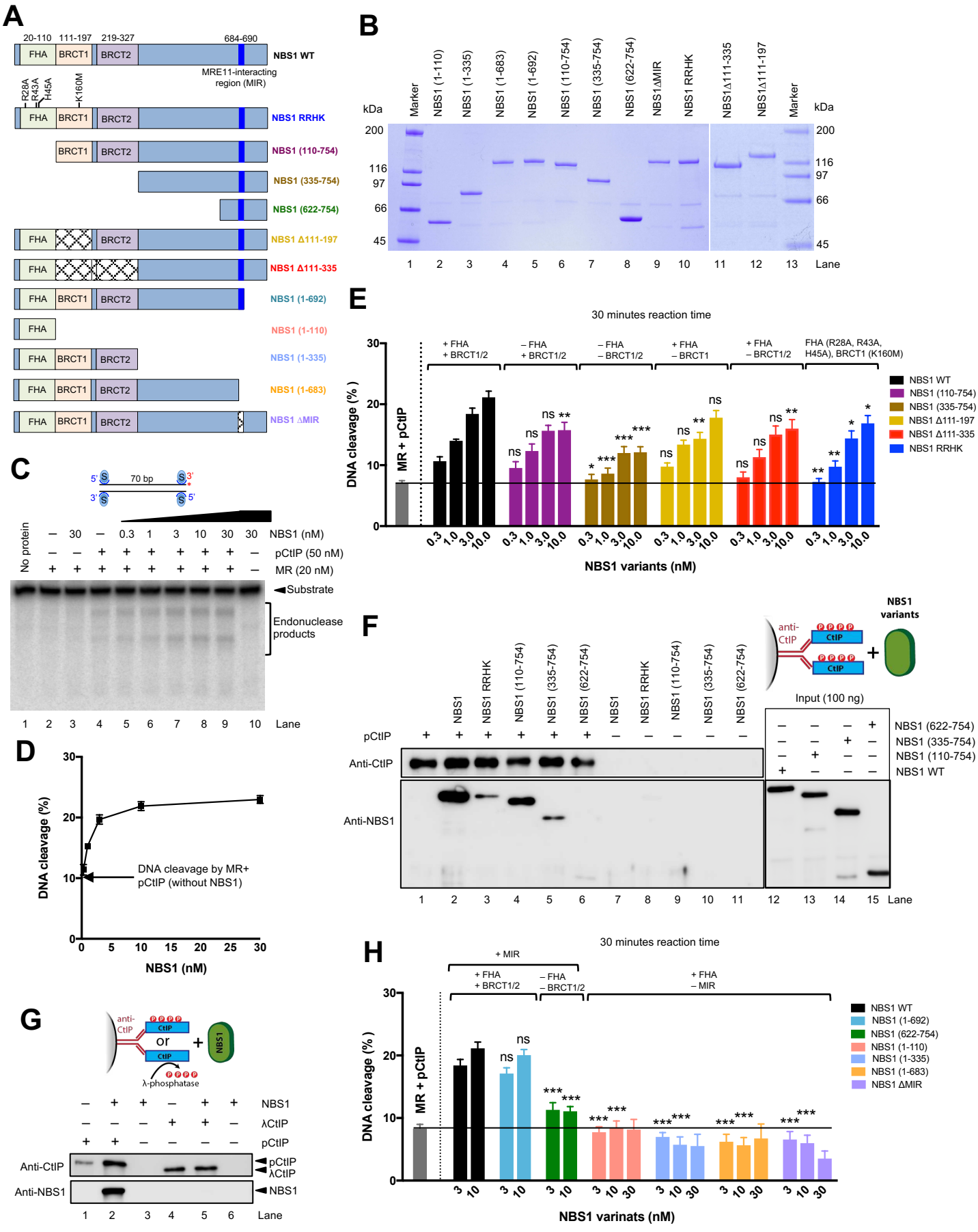
A
20-110
111-197
219-327
684-690
FHA
BRCT1
BRCT2
NBS1 WT
MRE11-interacting region (MIR)
R28A
R43A
H45A
K160M
NBS1 RRHK
NBS1 (110-754)
NBS1 (335-754)
NBS1 (622-754)
NBS1 Δ111-197
NBS1 Δ111-335
NBS1 (1-692)
NBS1 (1-110)
NBS1 (1-335)
NBS1 (1-683)
NBS1 ΔMIR
B
kDa
Marker
NBS1 (1-110)
NBS1 (1-335)
NBS1 (1-683)
NBS1 (1-692)
NBS1 (110-754)
NBS1 (335-754)
NBS1 (622-754)
NBS1ΔMIR
NBS1 RRHK
NBS1Δ111-335
NBS1Δ111-197
Marker
kDa
200
116
97
66
45
1 2 3 4 5 6 7 8 9 10 11 12 13 Lane
C
5' S 70 bp S 3'
3' S S 5'
No protein
NBS1 (nM) — 30 — 0.3 1 3 10 30 30
pCtIP (50 nM) — — + + + + + + —
MR (20 nM) + + + + + + + + —
Substrate
Endonuclease products
1 2 3 4 5 6 7 8 9 10 Lane
D
DNA cleavage (%)
DNA cleavage by MR+ pCtIP (without NBS1)
NBS1 (nM)
E
30 minutes reaction time
+ FHA + BRCT1/2
– FHA + BRCT1/2
– FHA – BRCT1/2
+ FHA – BRCT1
+ FHA – BRCT1/2
FHA (R28A, R43A, H45A), BRCT1 (K160M)
DNA cleavage (%)
MR + pCtIP
NBS1 WT
NBS1 (110-754)
NBS1 (335-754)
NBS1 Δ111-197
NBS1 Δ111-335
NBS1 RRHK
ns
*
**
***
0.3 1.0 3.0 10.0
NBS1 variants (nM)
F
NBS1 variants
anti-CtIP
CtIP
Input (100 ng)
pCtIP
NBS1
NBS1 RRHK
NBS1 (110-754)
NBS1 (335-754)
NBS1 (622-754)
Anti-CtIP
Anti-NBS1
NBS1 (622-754)
NBS1 (335-754)
NBS1 (110-754)
NBS1 WT
1 2 3 4 5 6 7 8 9 10 11 12 13 14 15 Lane
G
anti-CtIP
CtIP
or
NBS1
λ-phosphatase
NBS1
λCtIP
pCtIP
Anti-CtIP
Anti-NBS1
pCtIP
λCtIP
NBS1
1 2 3 4 5 6 Lane
H
30 minutes reaction time
+ MIR
+ FHA + BRCT1/2
– FHA – BRCT1/2
+ FHA – MIR
DNA cleavage (%)
MR + pCtIP
NBS1 WT
NBS1 (1-692)
NBS1 (622-754)
NBS1 (1-110)
NBS1 (1-335)
NBS1 (1-683)
NBS1 ΔMIR
ns
***
3 10 3 10 3 10 3 10 30 3 10 30 3 10 30 3 10 30
NBS1 varinats (nM)

Figure 3

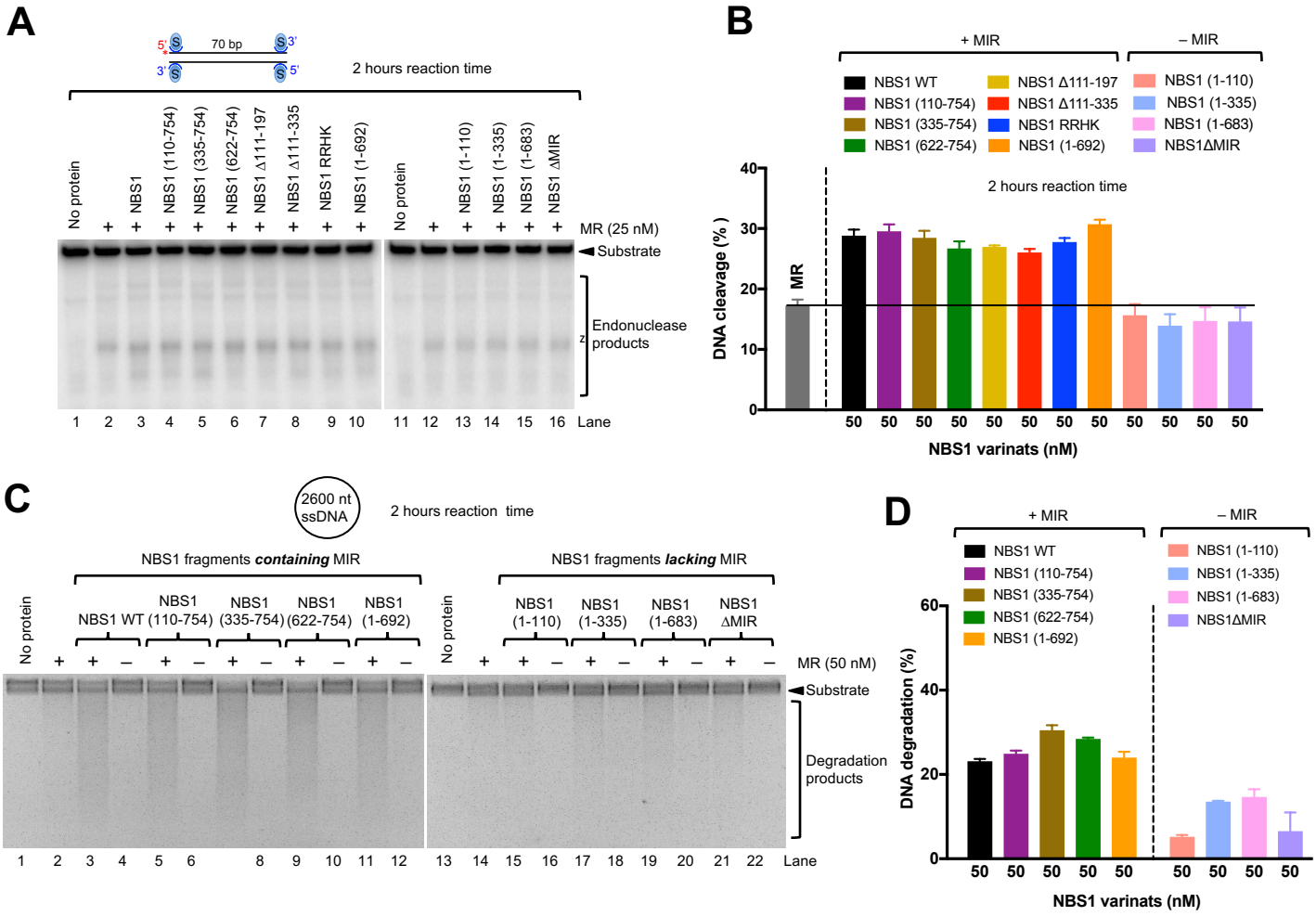
A
5′
3′
70 bp
3′
5′
2 hours reaction time
No protein
NBS1
NBS1 (110-754)
NBS1 (335-754)
NBS1 (622-754)
NBS1 Δ111-197
NBS1 Δ111-335
NBS1 RRHK
NBS1 (1-692)
No protein
NBS1 (1-110)
NBS1 (1-335)
NBS1 (1-683)
NBS1 ΔMIR
MR (25 nM)
Substrate
Endonuclease products
1 2 3 4 5 6 7 8 9 10 11 12 13 14 15 16 Lane
B
+ MIR
– MIR
NBS1 WT
NBS1 (110-754)
NBS1 (335-754)
NBS1 (622-754)
NBS1 Δ111-197
NBS1 Δ111-335
NBS1 RRHK
NBS1 (1-692)
NBS1 (1-110)
NBS1 (1-335)
NBS1 (1-683)
NBS1ΔMIR
2 hours reaction time
DNA cleavage (%)
MR
0 10 20 30 40
50 50 50 50 50 50 50 50 50 50 50 50
NBS1 varinats (nM)
C
2600 nt ssDNA
2 hours reaction time
NBS1 fragments ***containing*** MIR
NBS1 fragments ***lacking*** MIR
No protein
NBS1 WT
NBS1 (110-754)
NBS1 (335-754)
NBS1 (622-754)
NBS1 (1-692)
No protein
NBS1 (1-110)
NBS1 (1-335)
NBS1 (1-683)
NBS1 ΔMIR
MR (50 nM)
Substrate
Degradation products
1 2 3 4 5 6 8 9 10 11 12 13 14 15 16 17 18 19 20 21 22 Lane
D
+ MIR
– MIR
NBS1 WT
NBS1 (110-754)
NBS1 (335-754)
NBS1 (622-754)
NBS1 (1-692)
NBS1 (1-110)
NBS1 (1-335)
NBS1 (1-683)
NBS1ΔMIR
DNA degradation (%)
0 20 40 60
50 50 50 50 50 50 50 50 50 50
NBS1 varinats (nM)

Figure 4

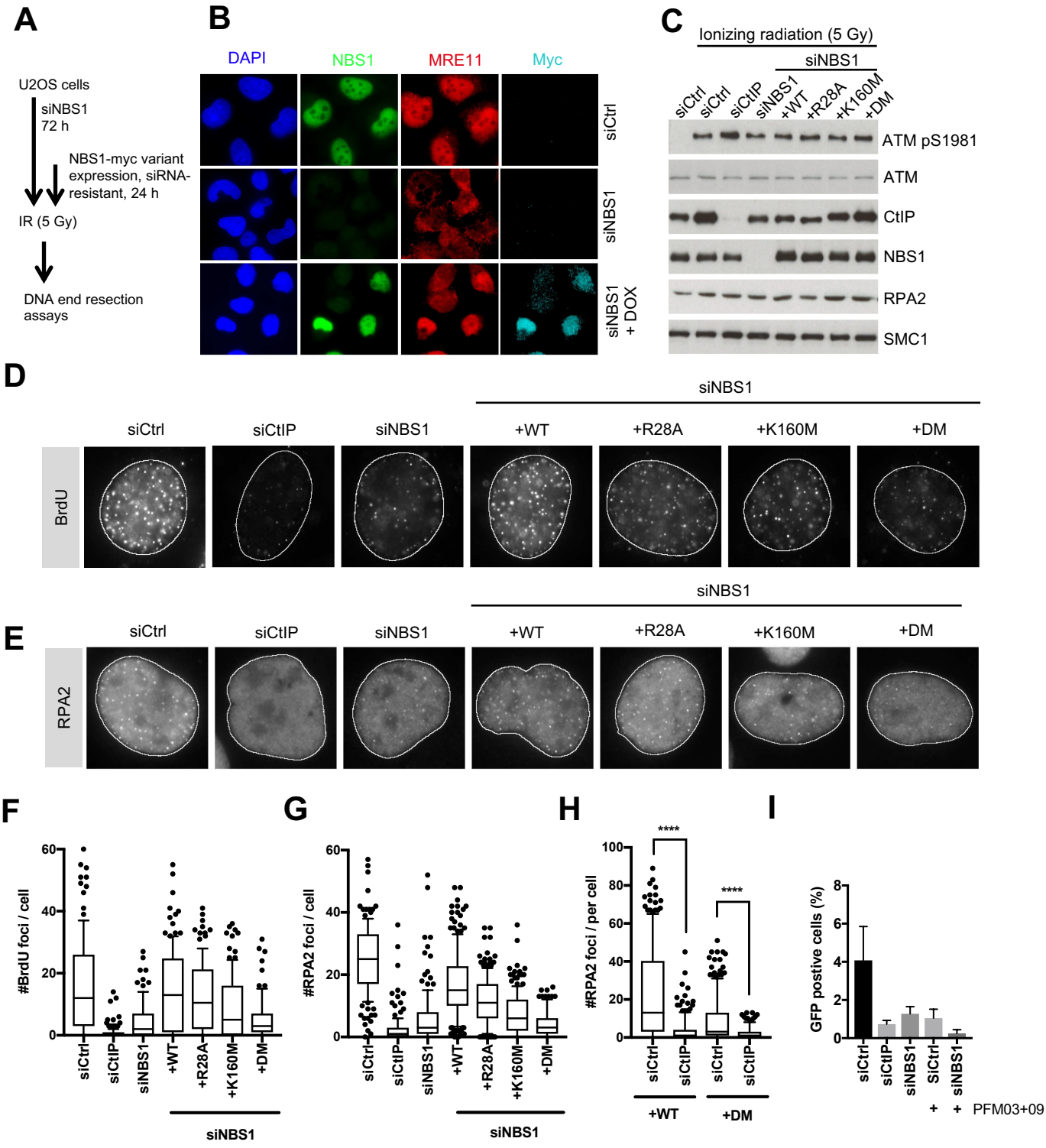
A
U2OS cells
siNBS1
72 h
NBS1-myc variant
expression, siRNA-
resistant, 24 h
IR (5 Gy)
DNA end resection
assays
B
DAPI
NBS1
MRE11
Myc
siCtrl
siNBS1
siNBS1
+ DOX
C
Ionizing radiation (5 Gy)
siNBS1
siCtrl
siCtrl
siCtIP
siNBS1
+WT
+R28A
+K160M
+DM
ATM pS1981
ATM
CtIP
NBS1
RPA2
SMC1
D
siNBS1
siCtrl
siCtIP
siNBS1
+WT
+R28A
+K160M
+DM
BrdU
E
siNBS1
siCtrl
siCtIP
siNBS1
+WT
+R28A
+K160M
+DM
RPA2
F
#BrdU foci / cell
siCtrl
siCtIP
siNBS1
+WT
+R28A
+K160M
+DM
siNBS1
G
#RPA2 foci / cell
siCtrl
siCtIP
siNBS1
+WT
+R28A
+K160M
+DM
siNBS1
H
#RPA2 foci / per cell
****
****
siCtrl
siCtIP
siCtrl
siCtIP
+WT
+DM
I
GFP postive cells (%)
siCtrl
siCtIP
siNBS1
SiCtrl
siNBS1
+
+
PFM03+09

Figure 5

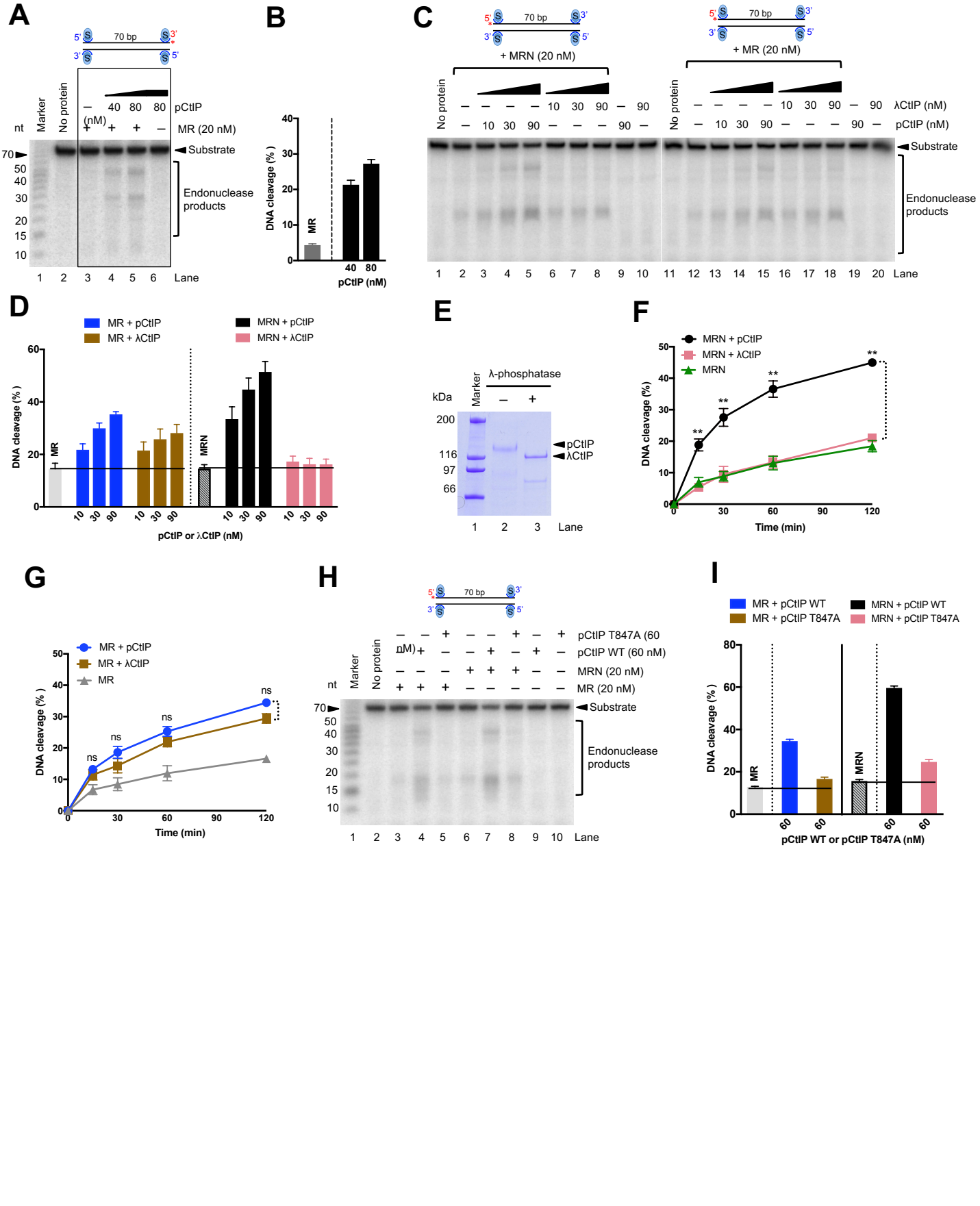
A
70 bp
Marker
No protein
pCtIP (nM)
MR (20 nM)
Substrate
Endonuclease products
nt
Lane
B
DNA cleavage (%)
MR
pCtIP (nM)
C
+ MRN (20 nM)
+ MR (20 nM)
λCtIP (nM)
pCtIP (nM)
D
MR + pCtIP
MR + λCtIP
MRN + pCtIP
MRN + λCtIP
pCtIP or λCtIP (nM)
E
λ-phosphatase
kDa
pCtIP
λCtIP
F
MRN + pCtIP
MRN + λCtIP
MRN
Time (min)
G
MR + pCtIP
MR + λCtIP
MR
ns
Time (min)
H
pCtIP T847A (60 nM)
pCtIP WT (60 nM)
MRN (20 nM)
MR (20 nM)
I
MR + pCtIP WT
MR + pCtIP T847A
MRN + pCtIP WT
MRN + pCtIP T847A
pCtIP WT or pCtIP T847A (nM)

Figure 6

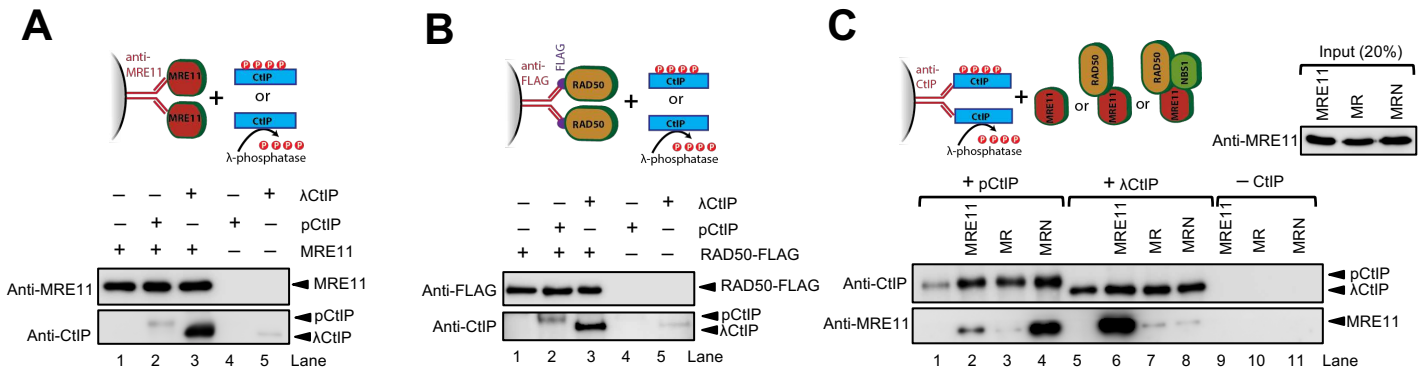
A
anti-
MRE11
MRE11
MRE11
CtIP
CtIP
or
λ-phosphatase
λCtIP
pCtIP
MRE11
Anti-MRE11
Anti-CtIP
MRE11
pCtIP
λCtIP
1 2 3 4 5 Lane
B
anti-
FLAG
RAD50
RAD50
CtIP
CtIP
or
λ-phosphatase
λCtIP
pCtIP
RAD50-FLAG
Anti-FLAG
Anti-CtIP
RAD50-FLAG
pCtIP
λCtIP
1 2 3 4 5 Lane
C
anti-
CtIP
CtIP
CtIP
λ-phosphatase
MRE11
or
RAD50
MRE11
or
RAD50
NBS1
MRE11
Input (20%)
MRE11
MR
MRN
Anti-MRE11
+ pCtIP
+ λCtIP
– CtIP
MRE11
MR
MRN
MRE11
MR
MRN
MRE11
MR
MRN
Anti-CtIP
Anti-MRE11
pCtIP
λCtIP
MRE11
1 2 3 4 5 6 7 8 9 10 11 Lane

Figure 7

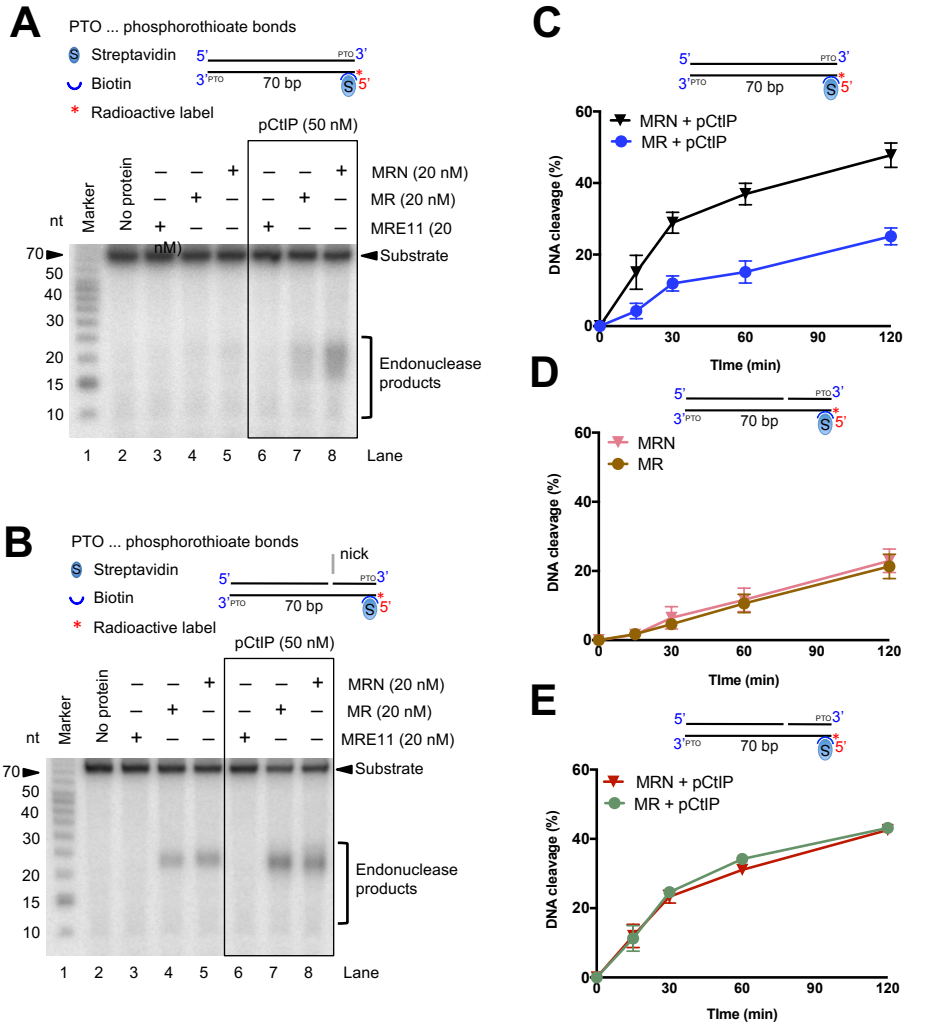
A
PTO ... phosphorothioate bonds
Streptavidin
Biotin
Radioactive label
5'
PTO 3'
3' PTO
70 bp
5'
pCtIP (50 nM)
Marker
No protein
MRN (20 nM)
MR (20 nM)
MRE11 (20 nM)
nt
70
50
40
30
20
15
10
Substrate
Endonuclease products
1 2 3 4 5 6 7 8
Lane
B
PTO ... phosphorothioate bonds
Streptavidin
Biotin
Radioactive label
nick
5'
PTO 3'
3' PTO
70 bp
5'
pCtIP (50 nM)
Marker
No protein
MRN (20 nM)
MR (20 nM)
MRE11 (20 nM)
nt
70
50
40
30
20
15
10
Substrate
Endonuclease products
1 2 3 4 5 6 7 8
Lane
C
5'
PTO 3'
3' PTO
70 bp
5'
MRN + pCtIP
MR + pCtIP
DNA cleavage (%)
60
40
20
0
0 30 60 90 120
TIme (min)
D
5'
PTO 3'
3' PTO
70 bp
5'
MRN
MR
DNA cleavage (%)
60
40
20
0
0 30 60 90 120
TIme (min)
E
5'
PTO 3'
3' PTO
70 bp
5'
MRN + pCtIP
MR + pCtIP
DNA cleavage (%)
60
40
20
0
0 30 60 90 120
TIme (min)

Figure 8

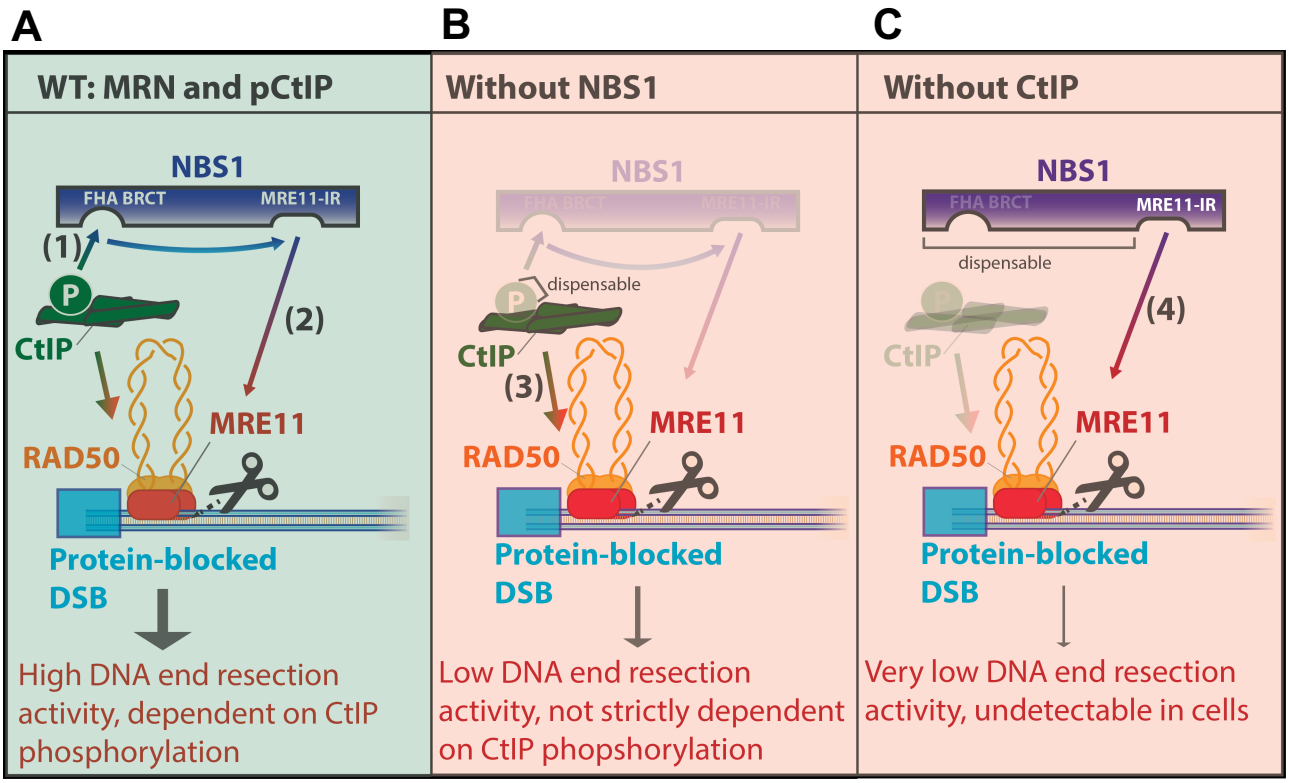
A
B
C
WT: MRN and pCtIP
Without NBS1
Without CtIP
NBS1
FHA BRCT
MRE11-IR
(1)
(2)
P
CtIP
MRE11
RAD50
Protein-blocked
DSB
High DNA end resection activity, dependent on CtIP phosphorylation
dispensable
(3)
Low DNA end resection activity, not strictly dependent on CtIP phopshorylation
(4)
Very low DNA end resection activity, undetectable in cells

Expandable view figure 1

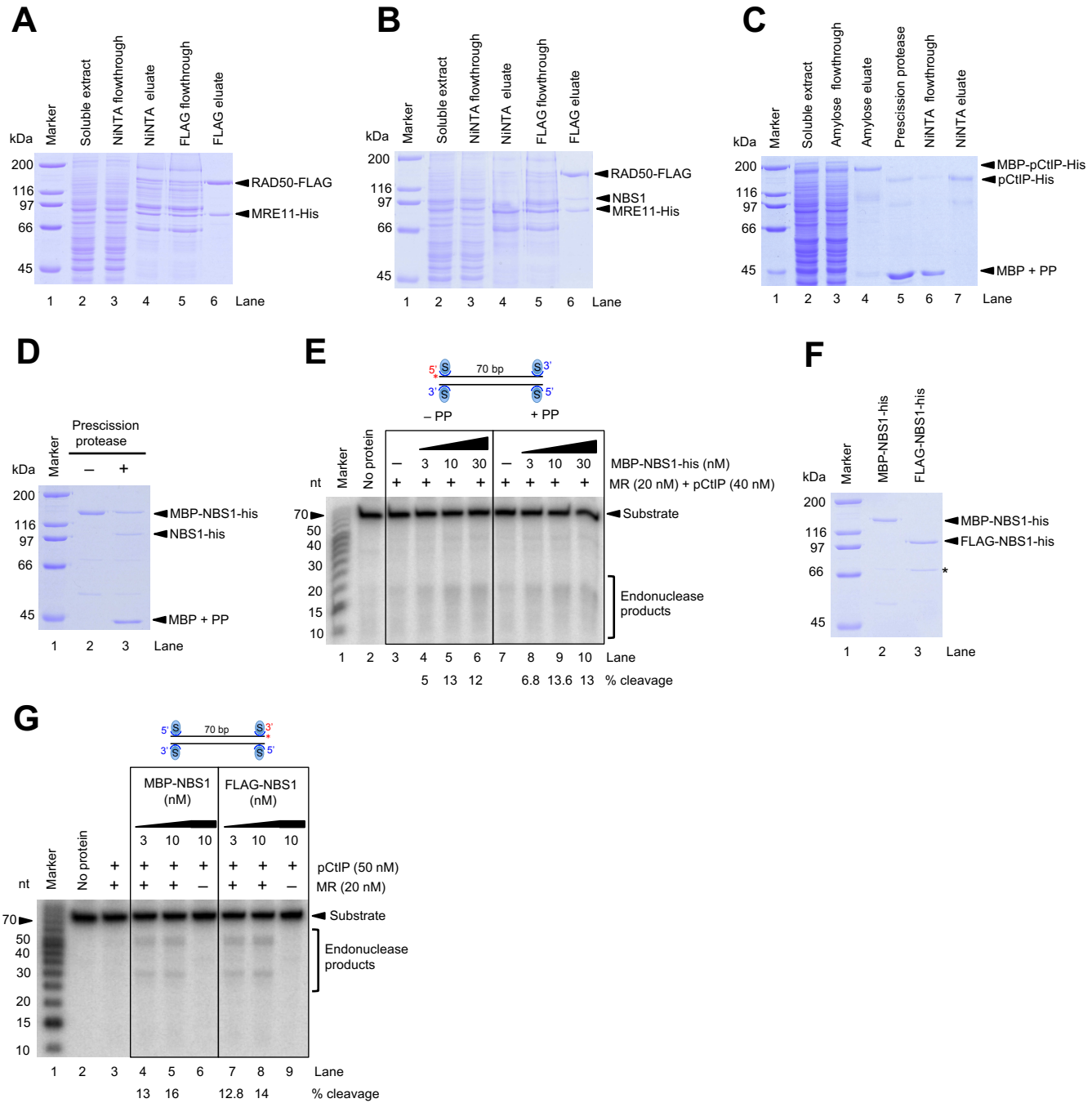

Expandable view figure 2

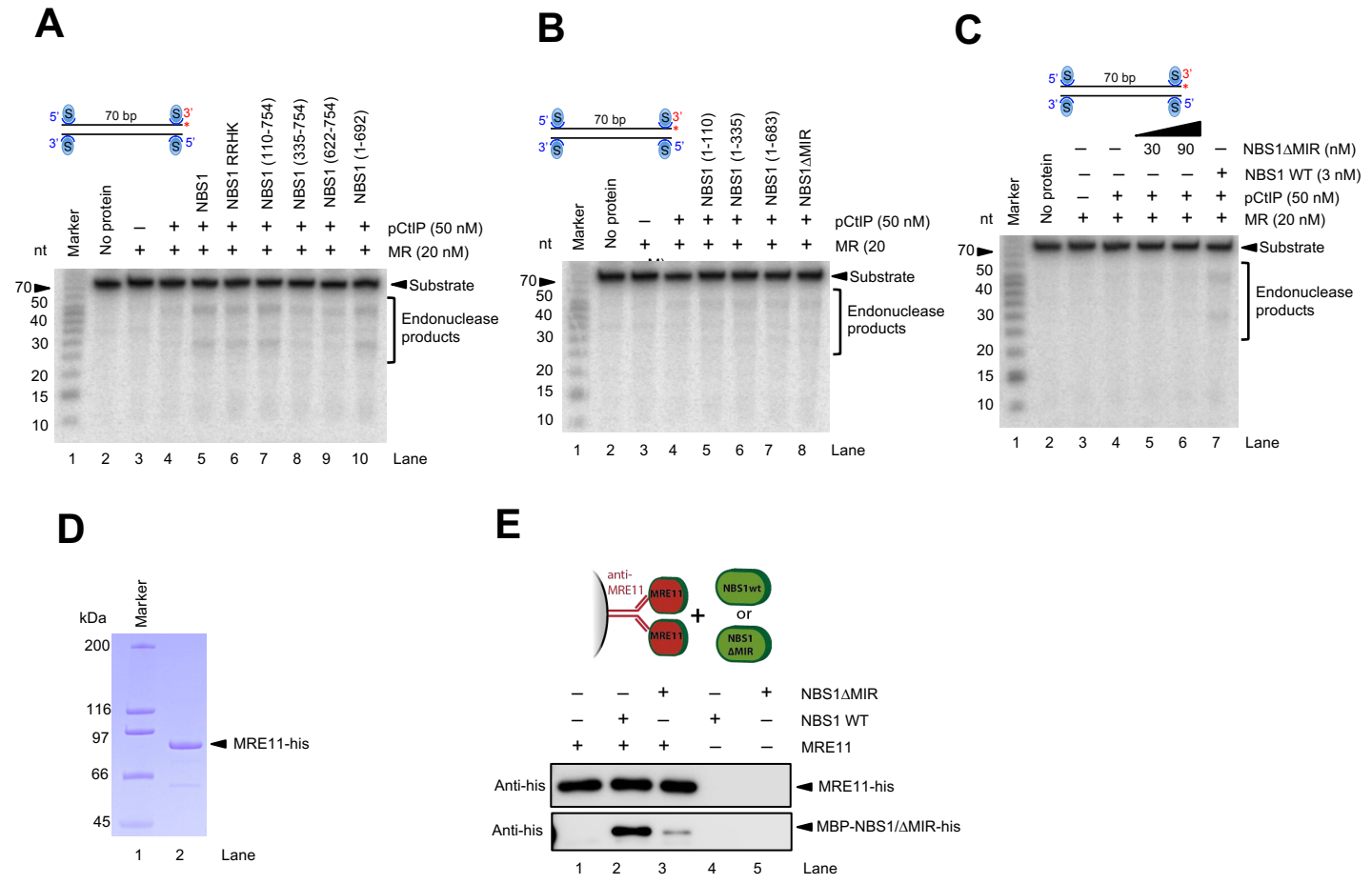

Expandable view figure 3

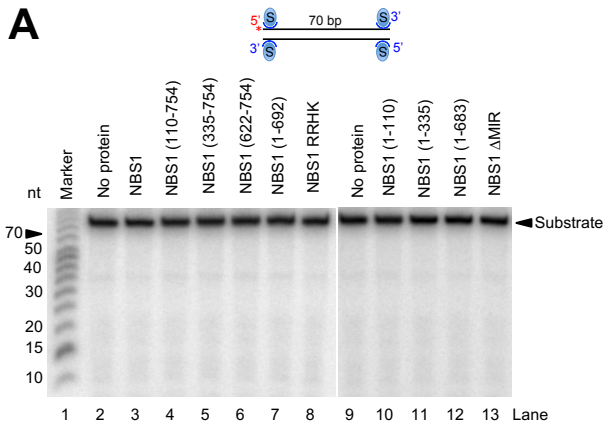

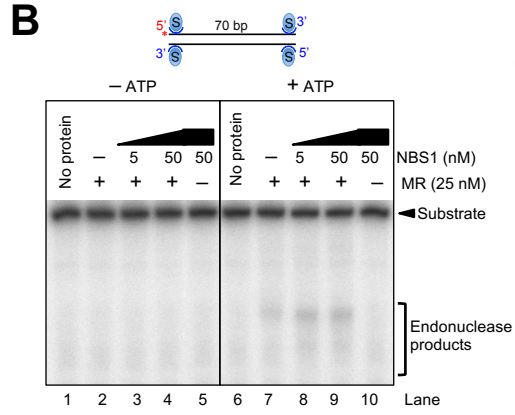

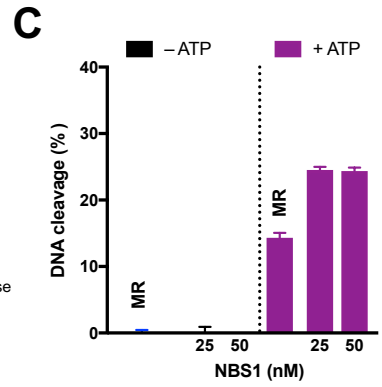

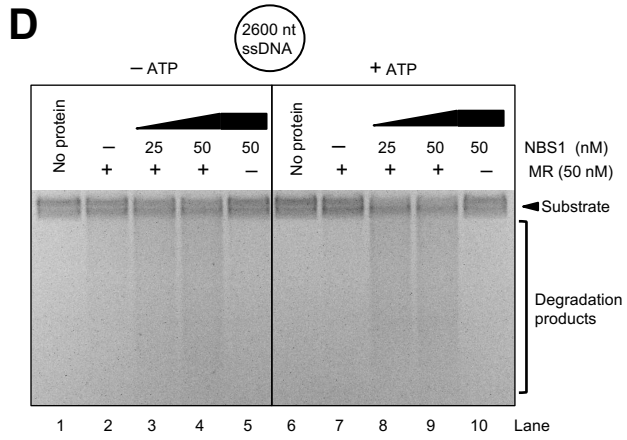

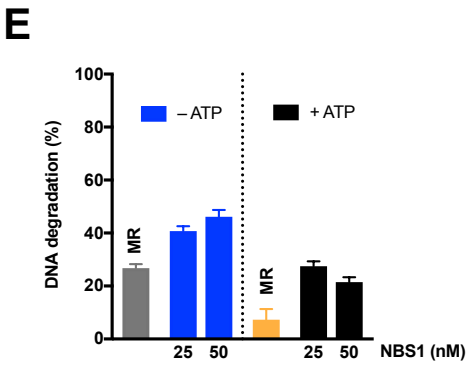

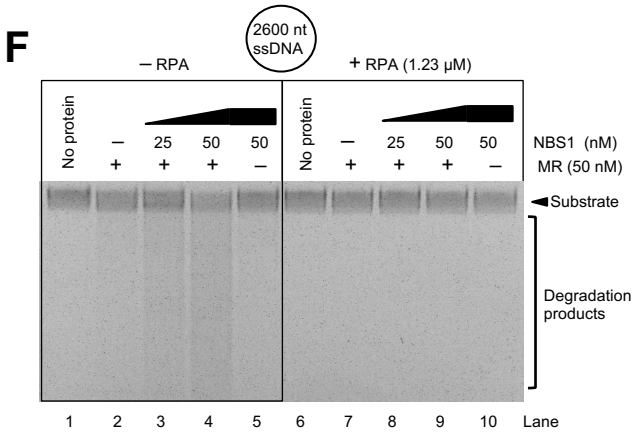

Expandable view figure 4

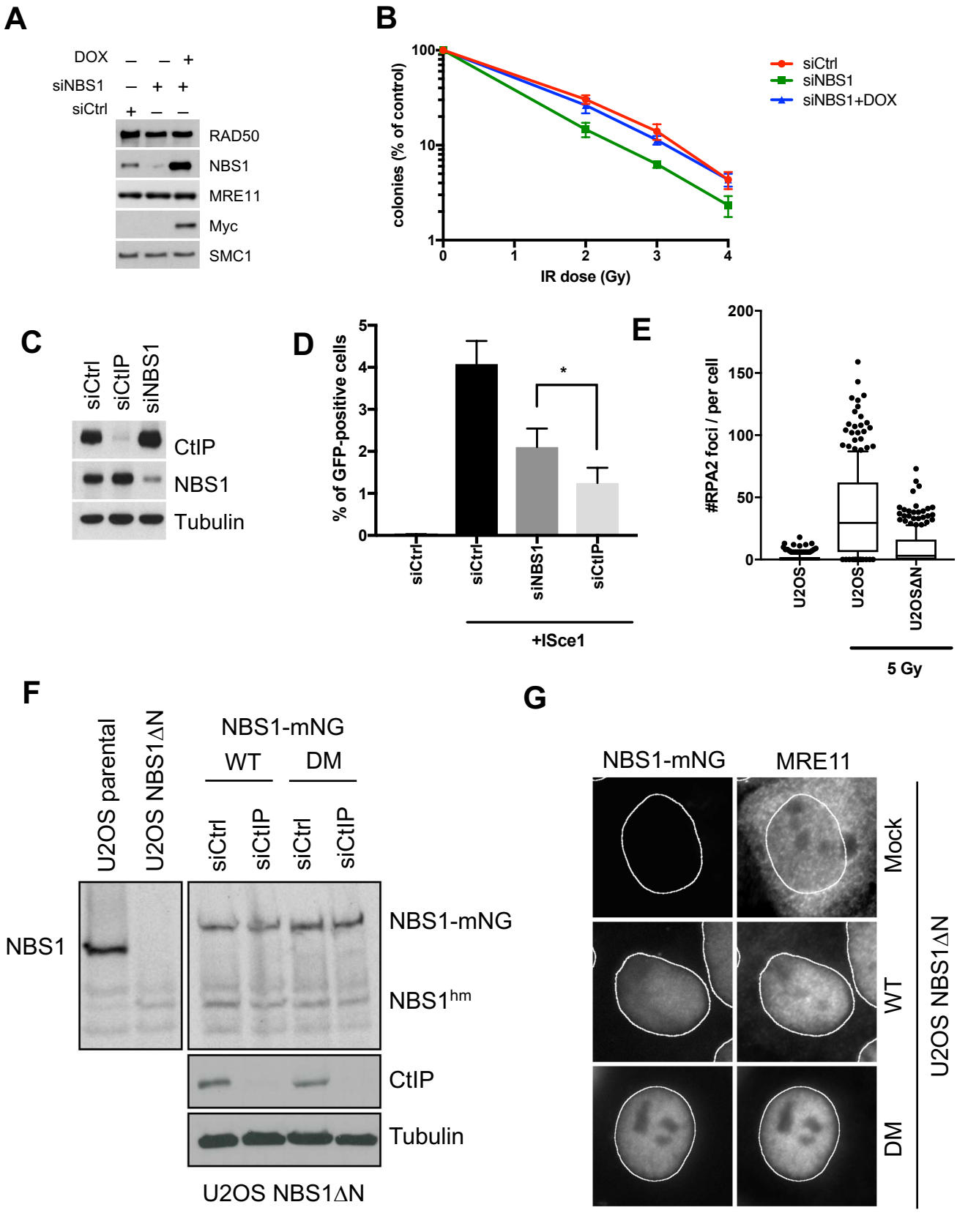

Expandable view figure 5

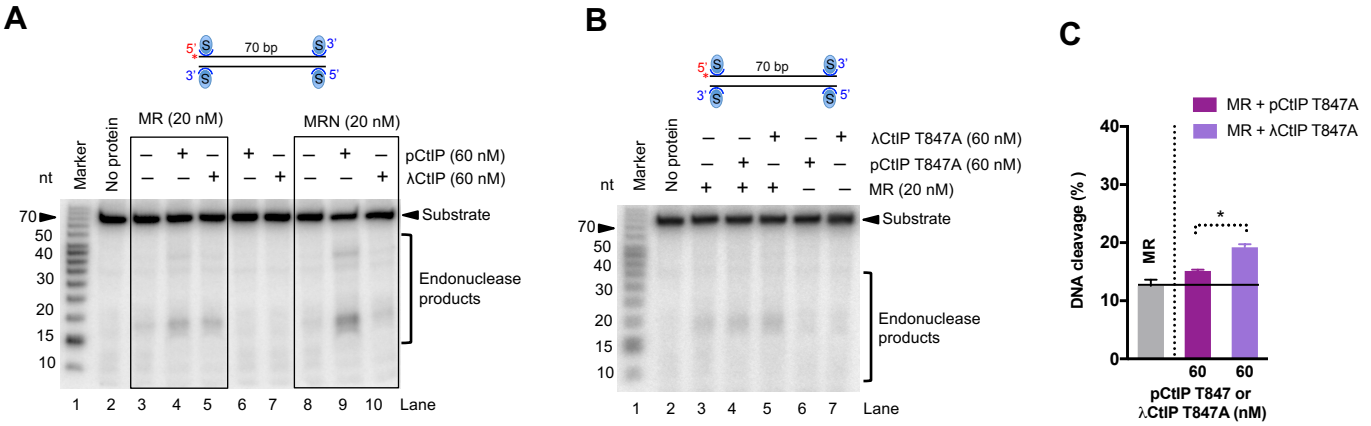

Expandable view figure 7